THESIS FOR THE DEGREE OF DOCTOR OF PHILOSOPHY

Power Consumption and Joint Signal Processing in Fiber-Optical Communication

Lars Lundberg

CHALMERS

Photonics Laboratory
Department of Microtechnology and Nanoscience (MC2)
CHALMERS UNIVERSITY OF TECHNOLOGY
Gothenburg, Sweden, 2019

Errata

”Power Consumption and Joint Signal Processing in Fiber-Optical Communication”

Lars Lundberg

March 11 2019

The following should be added to the printing location page:

ISBN 978-91-7905-103-7

Doktorsavhandlingar vid Chalmers tekniska högskola
Ny serie 4570
ISSN 0346-718X

Power Consumption and Joint Signal Processing in Fiber-Optical Communication

Lars Lundberg

Göteborg, March 2019

Chalmers University of Technology
Department of Microtechnology and Nanoscience
Photonics Laboratory
SE-412 96 Göteborg
Sweden
Telephone: +46 (0)31-772 10 00

Technical Report MC2-407
ISSN 1652-0769

Front cover illustration: Correlated phase noise from two channels in a frequency comb-based superchannel, with and without noticeable nonlinear phase noise. The launch-power value denotes the total launch power for 23 channels.

Printed in Sweden by Chalmers Digitaltryck, Chalmers tekniska högskola, 2019

Power Consumption and Joint Signal Processing in Fiber-Optical Communication

Lars Lundberg

Photonics Laboratory
Department of Microtechnology and Nanoscience
Chalmers University of Technology
SE-412 96 Göteborg, Sweden

Abstract

The power consumption of coherent fiber-optical communication systems is becoming increasingly important, for both environmental and economic reasons. The data traffic on the Internet is increasing at a faster pace than that at which optical network equipment is becoming more energy efficient, which means that the overall power consumption of the Internet is increasing. In addition, wasted energy leads to higher costs for network operators, through increased electricity expenses but also because the heat generated in the equipment limits how closely it can be packed.

This thesis includes both power consumption modelling and trade-off studies, as well as investigations of novel schemes for joint signal processing that may lead to an improved energy efficiency and increased performance in future systems. The power consumption modelling part includes a model of optical amplifier power consumption, which is connected to a performance model based on the Gaussian-noise model. Using these models, the trade-offs between amplifier power consumption and the choice of modulation format and forward-error-correction (FEC) scheme can be analyzed. Furthermore, the power consumption for a coherent link with minimal digital signal processing (DSP) is studied as well.

In the second part we investigate joint signal processing for phase-coherent superchannel systems based on optical frequency combs or multicore fiber. We find that the phase-coherence of optical frequency comb lines enables joint carrier recovery, which can increase performance and reduce the power consumption of the digital signal processing. The possible power consumption savings are quantified for a blind phase search method for phase tracking. Finally, we quantify the performance of joint carrier recovery for wavelength division multiplexed multicore fiber transmission in presence of nonlinear interference and inter-core skew.

Keywords: Fiber-optical communication, coherent detection, energy-efficiency, power consumption, optical amplifier, erbium-doped fiber amplifier, Raman amplification, digital signal processing, carrier-recovery, phase-tracking, optical frequency comb, multicore fiber, spatial division multiplexing

List of papers

This thesis is based on the following appended papers:

[A] **Lars Lundberg**, Peter A. Andrekson, and Magnus Karlsson, "Power Consumption Analysis of Hybrid EDFA/Raman Amplifiers in Long-Haul Transmission Systems," *Journal of Lightwave Technology*, vol. 35, no. 11, pp. 2132–2142, 2017.

[B] **Lars Lundberg**, Christoffer Fougstedt, Per Larsson-Edefors, Peter A. Andrekson, and Magnus Karlsson, "Power Consumption of a Minimal-DSP Coherent Link with a Polarization Multiplexed Pilot-Tone," in European Conference on Optical Communication (ECOC), 2016.

[C] **Lars Lundberg**, Magnus Karlsson, Abel Lorences-Riesgo, Mikael Mazur, Victor Torres-Company, Jochen Schröder, and Peter A. Andrekson, "Frequency Comb-Based WDM Transmission Systems Enabling Joint Signal Processing," *Applied Sciences*, vol. 8, no. 5, p. 718, 2018.

[D] **Lars Lundberg**, Mikael Mazur, Attila Fülöp, Victor Torres-Company, Magnus Karlsson and Peter A. Andrekson, "Phase Correlation Between Lines of Electro-Optical Frequency Combs," in Conference on Lasers and Electro-Optics (CLEO), 2018.

[E] **Lars Lundberg**, Erik Börjeson, Christoffer Fougstedt, Mikael Mazur, Magnus Karlsson, Peter A. Andrekson, and Per Larsson-Edefors, "Power Consumption Savings Through Joint Carrier Recovery for Spectral and Spatial Superchannels," in European Conference on Optical Communication (ECOC), 2018.

[F] **Lars Lundberg**, Mikael Mazur, Ali Mirani, Benjamin Foo, Jochen Schröder, Victor Torres-Company, Magnus Karlsson, and Peter A. Andrekson, "Phase-coherent lightwave communications with frequency combs," submitted to *Science*, 2019.

[G] **Lars Lundberg**, Benjamin J. Puttnam, Rubin S. Luís, Georg Rademacher, Magnus Karlsson, Peter A. Andrekson, Yoshinari Awaji, and Naoya Wada, "Master-slave carrier recovery for M-QAM multicore fiber transmission," submitted to *Optics Express*, 2019.

Papers by the author not included in the thesis:

[H] **Lars Lundberg**, Henrik Sunnerud, and Pontus Johannisson, "In-Band OSNR Monitoring of PM-QPSK Using the Stokes Parameters," in Optical Fiber Communication Conference (OFC), 2015, paper W4D.5.

[I] **Lars Lundberg**, Pontus Johannisson, Erik Agrell, Magnus Karlsson, and Peter A. Andrekson, "Power consumption of hybrid EDFA/Raman amplified systems," in European Conference on Optical Communication (ECOC), 2015.

[J] **Lars Lundberg**, Mikael Mazur, Abel Lorences-Riesgo, Magnus Karlsson and Peter A. Andrekson, "Joint Carrier Recovery for DSP Complexity Reduction in Frequency Comb-Based Superchannel Transceivers," in European Conference on Optical Communication (ECOC), 2017.

[K] Victor Torres-Company, Jochen Schröder, Attila Fülöp, Mikael Mazur, **Lars Lundberg**, Óskar Helgason, Magnus Karlsson and, Peter A. Andrekson, "Laser Frequency Combs for Coherent Optical Communications," *Journal of Lightwave Technology*, 2019.

Acknowledgment

First, I would like to thank my supervisors Prof. Peter Andrekson and Prof. Magnus Karlsson for accepting me as a PhD-student and guiding me through the process. I also gratefully acknowledge guidance from Prof. Erik Agrell, Dr. Pontus Johannisson, Prof. Per Larsson-Edefors, Dr. Jochen Schröder and Prof. Victor Torres-Company.

I would like to thank Dr. Naoya Wada for accepting me as a visiting PhD-student at the National Institute of Information and Communications Technology (NICT), Tokyo, Japan, and Dr. Ben Puttnam, Dr. Ruben Luís and Dr. Georg Rademacher for welcoming into the group there and helping me in the lab. I would also like to thank Dr. Tobias Eriksson for showing me around and for letting me borrow his fiber-scope.

My fellow project-member Christoffer Fougstedt deserves thanks for making me feel less lonely in this project, for teaching me about ASIC design and for generally being a friendly person. I would also like to acknowledge Erik Börjeson for being a very competent master thesis student (and now PhD student).

The experimental work in this thesis would not have been possible without Mikael Mazur, who also deserves thanks for his enthusiasm for fiber-optical communication and for always being friendly and helpful. Also Dr. Abel Lorences-Riesgo deserves thanks for helping me in the lab and being a nice office-mate. Another of my friendly former office-mates, Dr. Benjamin Foo, has helped me understand the behavior of nonlinear phase noise. Dr. Attila Fülöp helped me with DSP, frequency combs, and nerdy discussions. I would also like to thank Sheila Galt for support on everything teaching-related and Jeanette Träff for handling everything administrative in such a good way.

In addition, all the people at the Photonics lab deserve thanks for making it such a friendly workplace. I have been lucky enough to work in the same place as many new and old friends! Finally, I am grateful to all my friends and family for their company and support.

Lars Lundberg

Gothenburg
March 2019

This work was financially supported by the Knut and Alice Wallenberg foundation.

Abbreviations

ADC	Analog-to-digital converter
ASE	Amplified spontaneous emission
ASIC	Application-specific integrated circuit
AWG	Arrayed waveguide grating
BER	Bit-error rate
BPS	Blind phase-search
CD	Chromatic dispersion
CMA	Constant-modulus algorithm
COP	Coefficient of performance
CW	Continuous wave
DAC	Digital-to-analog converter
DBP	Digital back-propagation
DCF	Dispersion-compensating fiber
DD	Decision-directed
DEMUX	Demultiplexer
DSP	Digital signal processing
EDF	Erbium-doped fiber
EDFA	Erbium-doped fiber amplifier
EO	Electro optical
FBG	Fiber-bragg grating
FEC	Forward-error correction
FIR	Finite impulse-response
FWHM	Full-width half maximum
FWM	Four-wave mixing
GMI	Generalized mutual information
IQ	In-phase-quadrature
ISI	Inter-symbol interference
LD	Laser diode
LO	Local oscillator
MCF	Multi-core fiber
MIMO	Multiple-input multiple-output
MMA	Multi-modulus algorithm
MUX	Multiplexer
MZM	Mach-Zehnder modulator
NLI	Non-linear interference
OFDM	Orthogonal frequency division multiplexing
OSNR	Optical signal-to-noise-ratio
PBC	Polarization beam combiner
PBS	Polarization beam splitter
PMD	Polarization-mode dispersion
PPRN	Phase and polarization rotation noise
PSK	Phase-shift keying
QPSK	Quadrature phase-shift keying
RDE	Radius-directed equalization
RF	Radio-frequency
RX	Receiver
SDH	Synchronous digital hierarchy
SDM	Spatial-division multiplexing
SMF	Standard singlemode fiber
SNR	Signal-to-noise ratio
SONET	Synchronous optical networking
SPM	Self-phase modulation
TEC	Thermoelectric cooler
TIA	Transimpedance amplifier
TX	Transmitter
WDM	Wavelength-division multiplexing
XPM	Cross-phase modulation

Contents

Chapter 1

Introduction

As of the time of this writing, March 2019, it is estimated that more than half of the world's population are Internet users [1]. As such they are also users of fiber-optical communication, which is a technology crucial for the network infrastructure supporting the Internet. The usage of fiber-optical links ranges from underwater cables spanning thousands of kilometers, transporting data between continents, to high-capacity networks in the datacenters of service providers.

There are several inventions that have enabled fiber optical communication and the growth of data throughput in deployed systems. The low-loss optical fiber [2] and the laser [3] are fundamental for fiber-optical communication, and the invention of the erbium-doped fiber amplifier (EDFA) [4] extended the repeater-free reach and enabled the throughput to increase with wavelength-division multiplexing (WDM). More recently, coherent detection in combination with digital signal processing (DSP) [5] has enabled modulation formats with higher spectral efficiency. In addition, information theory, founded with Claude Shannon's landmark paper [6], as well as error control coding [7, 8] are fundamental for understanding the capacity of modern systems.

Altogether, the data rates of the installed systems have increased several orders in the last decades. Luckily enough, the power consumption of the equipment has not seen the same increase, which has enabled the energy consumption per transmitted bit and kilometer to decrease. For transatlantic cables, this decrease was estimated to be 20% annually [9]. However, the annual data traffic growth is estimated to be 40-50% [10], so the overall power consumption and energy use of the network infrastructure is increasing. There are several reasons to work to mitigate this trend. Maybe the most obvious one is the effects the use of fossil energy has on our planet [11], but there are also more pragmatical reasons to improve energy efficiency. Apart from

the obvious cost of energy that can be seen on any network operator's electricity bill, wasted energy takes the form of heat which requires cooling and set limits to how densely equipment can be packed [12]. Since space is a costly resource, this provides an additional incentive to improve energy efficiency.

This has created a need for a changed approach to development in the area of fiber optics. While the traditional approach has been to focus on performance and cost when designing systems, the systems of tomorrow need to be designed with an equal focus on power consumption. The work in this thesis contributes to this design paradigm.

1.1 Coherent technologies and joint signal processing

The focus of this work is on fiber-optical links using coherent detection. The strength of coherent detection is that it enables detection of the full optical field, which has the advantages that it enables the use of higher order modulation formats and that signal impairments can be compensated for with DSP. However, coherent transceivers have a significantly higher complexity and power consumption than transceivers for intensity-modulated signals. Therefore, coherent technologies have traditionally mainly been used in long-haul, high capacity links. Due to the large investments involved in e.g. submarine cables, and the relatively low number of installed links, the sensitivity to transceiver cost and power consumption is relatively low in this area. However, the use of coherent detection also in shorter links is on the rise—mainly in metro networks [13], but also in inter-datacenter interconnects [14]. These applications are more sensitive to cost and power consumption.

Over the last decade, it has been observed that the throughput demands for a single transceiver is increasing faster than the electrical bandwidth of the transceiver electronics [15, 16]. This has stimulated research related to so-called *superchannels* [17], which are a collection of traditional channels each modulated on a separate carrier [15]. This concept can include several technologies predicted to be important for future fiber optical communication systems. In the *spectral* domain, the frequency stability of optical frequency combs enables the sub-channels to be closely spaced, maximizing spectral efficiency. In the *spatial* domain, multicore and multimode fibers enable further scaling of the data throughput of single fiber [18]. Most importantly for the topic of this thesis, the fact that many channels are received in a single transceiver module introduces both new challenges and new possibilities. The challenges are that now many channels need to share the limited power allowed in a single module, and the possibilities are that the channels now can share components and resources between them. The latter opens up the possibilities for the second theme of this thesis, *joint signal processing*, which can reduce power consumption.

Joint signal processing is useful not only for power consumption savings, it can also be used to improve performance. Therefore, the joint signal processing methods discussed in this thesis are not limited to only power consumption savings.

1.2 This thesis

This thesis has two main, partly related topics. The first topic is power consumption in coherent fiber-optical communication systems. The overarching goal is to contribute to an increased energy efficiency of such systems. The second topic is joint signal processing, which can be used with the purpose of reducing power consumption, but also to enable performance gains. The papers included in this thesis falls into one or both topics. [Paper A–B] deals with modelling and understanding power consumption tradeoffs. [Paper C–G] are related to joint signal processing, either for power consumption savings or performance increase.

In [Paper A], the power consumption of optical amplifiers is modelled, and the tradeoff between power consumption and signal quality in terms of optical signal-to-noise ratio (OSNR) is investigated. The amplifier power consumption model includes both EDFAs and distributed Raman amplification. The connection between the OSNR and the power consumption enables analysis of the implications different modulation formats and forward error correction (FEC) schemes has on the amplifier power consumption.

In [Paper B] we investigate a minimal-DSP link, where length-dependent transmission impairments are absent, and polarization demultiplexing and carrier-recovery are aided by an optical pilot-tone.

[Paper C, D and F] covers the use of optical frequency combs in WDM-systems, and how the comb properties can be used in joint signal processing.

In [Paper E] we quantify possible power consumption savings enabled by master-slave carrier recovery, by an ASIC implementation of a blind phase search (BPS) based phase tracker, applicable to both spectral and spatial superchannels.

In [Paper G] we demonstrate master-slave carrier recovery in WDM multicore fiber transmission and investigate the effect of nonlinearities and inter-core skew on slave-channel performance.

1.2.1 Thesis outline

This thesis is organized as follows: Chapter 2 provides an overview over coherent fiber-optical communication systems and their power consumption, discussing how the basic building blocks and phenomena contribute to the power consumption. Chapter 3 is devoted to the power consumption of the two most common optical

amplification technologies, EDFAs and Raman amplification. We develop power consumption models from basic amplifier models and discuss system-wide trade-offs between amplifier power consumption and signal quality. In Chapter 4 the basic DSP functions needed in coherent systems are described, with extra attention given to carrier recovery. Chapter 5 introduces the concept of phase coherent superchannels, both in the spectral and spatial domain. The phase coherence properties of frequency combs are described in detail. This is followed by Chapter 6, where the principles and benefits of joint carrier recovery are described. Finally, Chapter 7 provides a future outlook.

Chapter 2

Principles of coherent fiber-optical communication

This chapter covers several aspects of coherent fiber-optical communication systems. The purpose is to provide an overview over the basic building blocks, their working principle and impact on system power consumption. In addition, we briefly discuss important transmission impairments, how they can be compensated for and the associated power consumption.

2.1 Building blocks

A telecommunication system, such as a fiber-optical link contains three essential parts: A *transmitter* that takes information and converts into a physical signal, a *transmission medium* that carries the signal, and a *receiver* that converts the signal back to usable data. In a fiber-optical link, the signal is carried on a lightwave, through an optical fiber, which is the transmission medium. However, the transmitter and receiver technology may differ between different kinds of fiber-optical systems.

In this thesis we consider coherent systems where the full optical field, i.e. both amplitude and phase on both polarizations is utilized to transmit information. The important building blocks of a coherent transmitter is the laser, which provides the carrier lightwave, and the modulator, which encodes the data onto the signal. Optical amplifiers can be considered to be part of the transmission medium. In the coherent receiver, the signal is detected with the help of a local oscillator (LO) laser and processed digitally to compensate impairments.

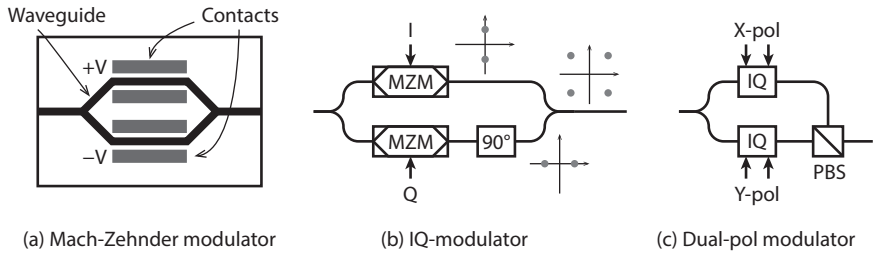

Figure 2.1: Principle of (a) an MZM (b) an IQ-modulator and (c) a dual-polarization IQ-modulator.

2.1.1 The laser

In coherent systems, a laser is needed both in the transmitter as a carrier and as an LO in the receiver. Typically, diode lasers are used. Important properties of lasers in coherent communication systems are output power, wavelength stability and linewidth. To assure wavelength stability, active cooling with thermoelectric coolers is used, which should be included when considering the power consumption. This is described in detail in Section 3.3. A tunable laser suitable for use in coherent systems can consume several watts [19], which is a considerable part of the transmitter power consumption [20]. However, in a transceiver, the same laser can often be used both as a carrier for the transmitter part and LO for the receiver part, thus sharing the power consumption.

2.1.2 The modulator

Coherent systems use optical in-phase-quadrature (IQ) modulators to modulate the full optical field. Although a single dual-drive Mach-Zehnder modulator can be used for quadrature modulation [21], to achieve independent modulation of the in-phase and quadrature dimensions, optical IQ-modulators are constructed with parallel Mach-Zehnder modulators (MZM). Mach-Zehnder modulators are based on placing two phase modulators in an interferometric structure, like in Figure 2.1(a). If opposite voltages are applied to the phase modulators, the amplitude of the output of the MZM can be modulated between -1 and 1 following the real axis in the transitions. To achieve modulation over the whole complex plane, two MZMs are combined with a 90° phase shift (Figure 2.1(b)). Finally, to modulate the full optical field, i.e. both polarizations, the output from two MZM-based IQ-modulators are combined with a polarization beam-combiner (PBC) (Figure 2.1(c)).

Important parameters for modulators are bandwidth, drive voltage and insertion losses, which are all related. The drive voltage is characterized by the voltage to

achieve a phase shift of 180° (or π) in the child phase modulators, written V_π. For the MZM described above, this corresponds to the voltage needed to go between -1 and 1. High-speed phase modulators are often based on the travelling-wave design [22, Ch. 2], where the electrodes are designed as a transmission line alongside the optical waveguide. In a travelling-wave modulator, the light is modulated as it travels through the waveguide. To lower the V_π it is desirable to have a long interaction length between the electrical signal and the light, but due to difference in propagation speed between the electrical signal and the light, a long interaction length will reduce the modulation bandwidth of the modulator [22, Ch. 2]. In addition, long interaction lengths will increase losses both in the electrical transmission line and the optical waveguide [23].

The power consumption of the modulator has two main components. First, high insertion losses require high optical power from the transmitter laser, or even booster amplifiers. Second, a high drive voltage leads to a high electrical power consumption. The electrical power is not consumed in the modulation process itself, but is rather dissipated in the 50 Ω terminations or in transmission line losses, and is proportional to V_π^2. In [20], it is estimated that the modulator contributes with around 35% of the total transmitter power consumption.

Modulators can be constructed from several different materials, but the most established today is lithium-niobate ($LiNbO_3$), where phase-modulation is achieved through the electro-optic effect. Another possible material is indium phosphide (InP). Modulators based on InP can be integrated with other InP optical components, such as tunable lasers, receivers and arrayed waveguide gratings [24].

2.1.3 The optical amplifier

To manage fiber losses optical amplification is used, most commonly in the form of lumped erbium-doped fiber amplifiers (EDFAs). The optical amplifiers are also the most important noise source, as they inherently add amplified spontaneous emission (ASE) noise to the signal. The EDFAs are inserted with a spacing of between 50 km and 100 km. Alternatively, the transmission fiber itself can be used as amplification medium through stimulated Raman scattering. Since the amplification takes place along the transmission fiber, this is referred to as distributed amplification. The main reason for using Raman amplification is its beneficial noise properties. Optical amplifiers are covered in more detail in Chapter 3.

2.1.4 The coherent receiver

Today, the term coherent receiver usually refers to a phase- and polarization-diversity coherent receiver, that can detect both phase and amplitude of the optical field. Fig-

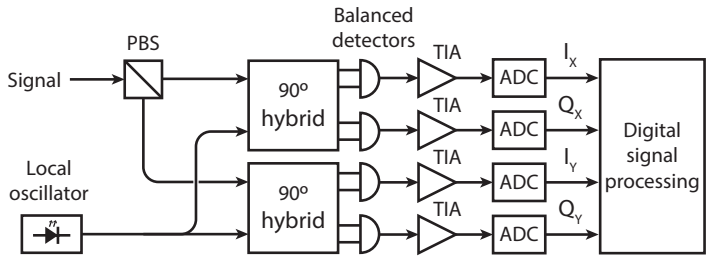

Figure 2.2: A phase- and polarization-diversity coherent receiver.

ure 2.2 shows a schematic of such receiver. The optical signal is split into orthogonal polarization states with a polarization beam splitter (PBS) and each of the polarizations is mixed with an LO laser in a 90° hybrid. The signal and LO are detected with balanced photodetectors. Typically, the receiver is operated in intradyne mode, which means that the LO laser is kept at approximately, but not exactly, the same frequency as the signal. Then there will be a remaining frequency difference between the signal and the LO that needs to be tracked using digital signal processing.

The signal from the photodetectors can be amplified with transimpedance amplifiers (TIAs) before analog-to-digital conversion. Power consumption of photodiode bias and TIAs are comparably small parts of the total receiver power consumption [20].

2.1.5 Analog-to-digital conversion

The analog-to-digital converters (ADCs) are responsible for converting the analog signal from the balanced detectors to fixed-point digital signals suitable for digital signal processing (DSP). For fiber-optical systems, the most suitable technology is based on time-interleaved successive approximation [25]. The power consumption of this ADC technology is approximately linearly dependent on the sampling rate, and the ADC bit resolution, which determines the number of quantization levels [26].

2.1.6 Digital signal processing

The DSP is an essential part of coherent optical communication systems, and a major power consumer in the receiver. Chapter 4 covers DSP in detail.

2.1.7 Forward error correction

Often, a signal is consider error free if the bit-error rate (BER) is below 10^{-15}. To achieve such low BERs, modern fiber optical communication systems rely on forward error correction (FEC), where a small redundancy added to the signal is traded against a significantly higher tolerance to noise and other impairments. FEC codes require encoding and decoding that may consume considerable amounts of power [20, 27].

There are two main categories of error-correcting codes, hard-decision codes and soft-decision codes. Hard-decision codes are decoded after a symbol decision has been made, while soft-decision codes perform decoding based on soft information about the received samples. Typically, soft-decision codes have a higher error-correcting capability at the cost of a higher decoding complexity and power consumption.

The overall trend is that a higher error-correcting capability leads to a higher power consumption. Since the power consumption of the line amplifiers can be reduced if the OSNR is lower, there is possibly a trade-off between the FEC power consumption and the power consumption of the amplifiers. Indeed, in [Paper A] we find that there are cases where the combined FEC and amplifier power consumption can be lowered by using a more powerful FEC and operating the system at a lower OSNR. However, specific details of the code type, design and implementation has also a big impact on the power consumption, so one should be careful before drawing to wide conclusions from this example.

2.2 Signal impairments

There are many sources of impairments in coherent fiber-optical communication systems. They can roughly be divided into three categories: Impairments caused by non-ideal transmitter and receiver components, linear transmission impairments, and nonlinear transmission impairments. The first category includes limited bandwidth of electrical components, limited resolution of DACs and ADCs, bias errors in the modulator and phase noise of the carrier and LO lasers. This section will discuss laser phase noise and transmission impairments in more detail.

2.2.1 Laser phase noise

With a free-running LO, the different center frequencies of the transmitter and LO lasers will cause the detected signal to have remaining frequency offset. In addition, the lasers have a finite linewidth, which means that their phases will fluctuate. Laser

phase noise is commonly modelled as a Wiener process

$$\theta_k = \theta_{k-1} + \Delta_k, \tag{2.1}$$

where θ_k is the phase of the k-th sample, and the Δ_k is a real random Gaussian variable with zero mean and variance

$$\sigma_\theta^2 = 2\pi\Delta f T_s. \tag{2.2}$$

Here Δf is the combined laser linewidth of the transmitter and LO laser and T_s is the time between phase samples.

2.2.2 Chromatic and polarization-mode dispersion

The origin of chromatic dispersion is the frequency dependence of the propagation constant in the fiber. This is caused by a combination of material dispersion and waveguide dispersion. Chromatic dispersion leads to inter-symbol interference (ISI) and if it is not compensated for, it severely limits the transmission reach. Compensation can be performed both in the optical domain or electronically using DSP. The most common optical method is dispersion-compensating fiber (DCF), which has been designed to have a dispersion parameter with an opposite sign to that of standard single mode fiber (SMF). Another method is fiber Bragg gratings (FBG). Optical dispersion compensation contributes to the power consumption by introducing losses that need to be compensated with optical amplification [28]. Since FBGs have lower losses than DCF [29], they are a more power efficient choice. DSP-based electronic dispersion is covered in more detail in Section 4.1.2. If used, it is one of the major power consumers in the receiver [20].

Polarization-mode dispersion (PMD) is caused by fiber birefringence, which leads to a polarization dependent propagation constant. The origin of the birefringence is small deviations of the fiber core geometry along the fiber. Since the effect PMD has on the signal varies depending on the polarization, and the polarization drifts with time, PMD is a time dependent impairment. From a signal processing point of view, PMD causes a frequency dependent crosstalk between the polarizations, and can thus be compensated for with a 2×2 MIMO-equalizer. Since PMD varies with time, this equalizer needs to be adaptive.

2.2.3 Non-linear impairments

In addition to the previously discussed linear impairments, there are also non-linear impairments from the power dependence of the refractive index of the optical fiber. The refractive index of optical fiber has a quadratic dependence on optical power,

which is known as the Kerr effect. Since the light is highly confined in the core over long distances, non-linear effects are important even though silica is not highly non-linear. Through the power dependence of the refractive index, the signal will distort itself through self-phase modulation (SPM) and interact with other wavelength channels and noise through cross-phase modulation (XPM) and four-wave mixing (FWM). Of these three effects, FWM is less significant in transmission links using SMF due to the dispersion of the fiber.

The effect of interchannel nonlinear impairments can be described in terms of three contributions: One that behaves as additive Gaussian noise, one that causes phase variation, and one that causes polarization rotations [30, 31]. The latter ones can be grouped together and referred to as phase and polarization rotation noise (PPRN). The importance of PPRN depends on the modulation format of the interfering channels, with modulation formats with many amplitude levels giving a stronger PPRN contribution [30, 31]. Furthermore, unlike Gaussian noise, PPRN has a relatively long temporal correlation, which means that it can be tracked by an equalizer in the receiver [31–33]. While ideally, a MIMO equalizer with several taps should be used to capture both polarization rotations and frequency dependence, a standard phase noise tracking algorithm will be able to track parts of the PPRN [34, 35].

The *Gaussian-noise model* or *GN model* is a model for nonlinear interference that is based on the assumption that in long-haul links without inline dispersion compensation, nonlinear effects can often be treated as additive Gaussian noise [36, 37]. The reason for this description to be valid is that the signal distortion caused by chromatic dispersion causes the nonlinear interference to resemble Gaussian noise. However, this ignores the PPRN contributions of nonlinearities, but due to its simplicity to use the GN-model is a common way to estimate performance. The underlying theory has been described in e.g. [36, 37]. The fundamental result is that an additional noise term with spectral density S_{NLI} proportional to the cube of signal power is added to the noise power spectral density. The optical signal-to-noise ratio (OSNR) is then

$$\mathrm{OSNR} = \frac{P_s}{(S_{\mathrm{ASE}} + S_{NLI})\Delta\nu} = \frac{P_s}{(S_{\mathrm{ASE}} + k_{\mathrm{NLI}} P_s^3)\Delta\nu}, \tag{2.3}$$

where P_s is the signal launch power, S_{ASE} is the amplifier noise power spectral density, $\Delta\nu$ is the noise bandwidth (usually corresponding to 0.1 nm) and k_{NLI} is a proportionality constant that depends on fiber properties and signal spectra of the whole system.

Using this model an expression for the optimal signal power that gives the highest OSNR can be calculated, which is when ASE and nonlinearities balance each other.

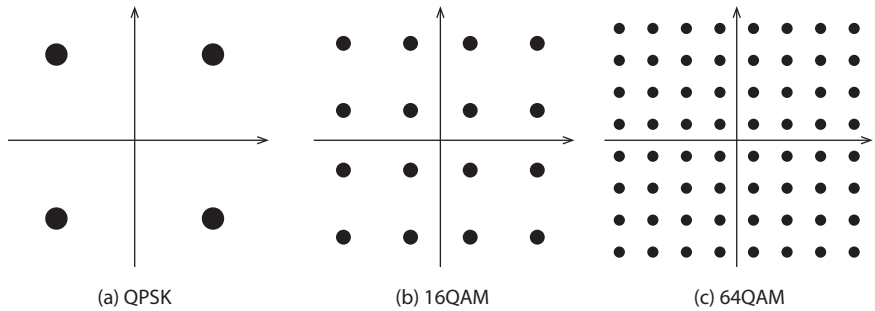

Figure 2.3: Constellations of three modulation formats.

This optimum is given by

$$P_{\text{opt}}^{s} = \left(\frac{S_{\text{ASE}}}{2k_{\text{NLI}}} \right)^{1/3}. \tag{2.4}$$

This expression is in many cases used in combination with the Shannon capacity as a measure of the maximum possible capacity of a fiber system. However, this is not actually the capacity of the fiber channel. Rather it is a lower bound on it [38], whereas the actual capacity of the fiber channel remains unknown.

2.3 Modulation formats

Coherent transmission enables the use of quadrature amplitude modulation (QAM) formats, illustrated in Figure 2.3. Quadrature phase-shift keying (QPSK, or 4QAM) and 16QAM is today available in commercial coherent transceivers [12], and even higher order formats are expected to be available in the future.

The choice of modulation format affects the power consumption in several ways. Higher order modulation formats are more sensitive to noise, which may lead to higher power consumption in amplifiers [Paper A] and FEC. They also require higher bit-resolution which increase power consumption of ADCs and all DSP. In addition, higher order modulation formats are also more sensitive to impairments such as phase noise and thus require more complex phase-tracking algorithms. However, due to the increased spectral efficiency, the power consumption per bit may be unaffected or even lowered [20, 27], [Paper A].

2.4 Performance metrics

The bit-error-rate (BER) is maybe the most straight-forward performance metric and is as the name implies simple the ratio of the number of bits received in error and the total number of received bits. However, the end-to-end BER, after error-correction, can be challenging to estimate. One reason is that it would take unacceptably long time to reach the number of bit-errors required for statistically significant results in systems with offline DSP and simulated systems. The other reason is that often experiments and simulations do not include FEC, to not be limited to a specific code or implementation. Therefore, a way of predicting the post-FEC performance of a system based on the received signal before FEC is highly desirable. For hard-decision FEC codes, the post-FEC BER is often well predicted by the pre-FEC BER, which has led to the common usage of the so-called FEC-limit or FEC-threshold, which denotes the acceptable pre-FEC BER to achieve a low enough post-FEC BER.

However, despite being used often, for soft-decision codes, pre-FEC BER is a poor predictor for post-FEC BER [39]. An alternative metric is the generalized mutual information (GMI) [39]. The GMI predicts the maximum possible data throughput taking FEC overhead into account, using bit-wise decoding. When bit-wise decoding is used, the symbols are detected before decoding, and the bits are assigned with soft-information [39]. This is a structure is commonly used in optical receivers employing soft-decision FEC. The GMI is measured in bits per symbol, and has a maximum value depending on the modulation format. It can be measured per 2D-symbol for single polarization or per 4D-symbol for dual polarization signals. However, GMI as a measure has the drawback that it assumes codewords of infinite length, which is not possible in reality. Therefore GMI should be regarded as an upper bound on a real FEC implementation [40].

Chapter 3

Power consumption of optical amplifiers

Optical amplifiers are a fundamental part of long-haul optical communication systems and a major power consumer [20]. They are also the most important noise source, and the choice of amplification scheme has significant impact on the signal quality at the receiver. To be able to investigate the trade-offs between signal quality and power consumption, the whole system needs to be considered when modelling amplifier power consumption. In this chapter the power consumption of the two most common optical amplification technologies, erbium-doped fiber amplifiers (EDFAs) and distributed Raman amplification, is described starting from fundamental amplifier models.

Both EDFAs and Raman amplifiers have in common that they provide optical gain by pumping an amplification medium with a high-power optical wave. While EDFAs use erbium-doped fiber (EDF) as amplification medium, Raman amplification can be achieved in standard single mode fiber (SMF). Parts of the power consumption of optical amplifiers is directly proportional to the pump power, so the following sections will be spent connecting the required pump power to other important amplifier properties such as gain and output power.

3.1 Erbium-doped fiber amplifiers

The erbium-doped fiber amplifier is the dominant amplifier technology used in long-haul fiber-optical communication systems. The amplification is achieved through

stimulated emission, which is the process where a photon stimulates an atomic energy transition. The energy is released in the form of a photon with identical wavelength, phase, polarization and propagation direction as the incident photon. Er^{3+} ions are used since they have an atomic energy transition matching the telecommunication wavelength of 1550 nm. To provide gain, there must be population inversion, i.e., most of the ions need to be in the excited state.

In amorphous silica, the energy levels of the Er^{3+} ions are broadened to bands, providing gain over both the C- and L-band (1530–1565 nm and 1565–1625 nm respectively). Population inversion can be achieved by optical pumping, either at 980 nm or at 1480 nm. Pumping at 980 nm corresponds to a third energy level, while 1480 nm corresponds to the upper parts of the same energy band that is providing amplification.

3.1.1 Fundamental limits

The efficiency with which the pump power is converted into signal power is fundamentally limited by photon number conservation, i.e., the most efficient case corresponds to when all pump photons are converted into signal photons. Then, the photon flux (the number of photons per second) at the output needs to equal the photon flux at the input, giving

$$\Phi^s_{\text{out}} = \Phi^s_{\text{in}} + \Phi^p_{\text{in}}, \tag{3.1}$$

where Φ^s_{out} and Φ^s_{in} are the photon fluxes of the signal at the output and input of the amplifier and Φ^p_{in} is the photon flux of the pump at the input. By observing that the photon flux can be written in terms of the optical power P as $\Phi = P\lambda/(hc)$, where λ is the optical wavelength, h is the Planck constant and c is the speed of light, this equation can be rewritten

$$P^p_{\text{in}} = \frac{\lambda_s}{\lambda_p}(P^s_{\text{out}} - P^s_{\text{in}}), \tag{3.2}$$

where P^s_{out} and P^s_{in} are the signal powers at the output and input of the amplifier, P^p_{in} is the pump power at the input, and λ_s and λ_p are the signal and pump wavelengths respectively. This shows that if all pump photons are converted to signal photons, the pump power needed will be proportional to the power added to signal. The maximum efficiency corresponds to the ratio between the pump and signal wavelengths. Assuming a signal wavelength of 1550 nm, this corresponds to a power conversion efficiency of 63% and 95% for pump wavelengths of 980 nm and 1480 nm respectively.

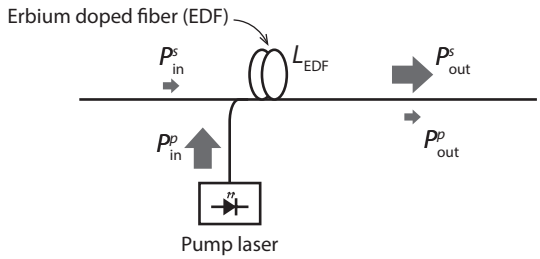

Figure 3.1: Schematic of a basic EDFA, with one co-propagating pump.

Despite its simplicity, as we will show in the next section, the general behavior of the pump and signal power dependence is well described by this model for typical uses of EDFAs in communication links, provided that the wavelength ratio is replaced with a non-ideal power conversion efficiency η_{PC}. The model then becomes

$$P^p_{\text{in}} = \frac{1}{\eta_{\text{PC}}}(P^s_{\text{out}} - P^s_{\text{in}}) \quad \text{where} \quad \eta_{\text{PC}} < \frac{\lambda_p}{\lambda_s}. \tag{3.3}$$

We will refer to this model as the *added-power model*. Introducing the amplifier gain $G = P^s_{\text{out}}/P^s_{\text{in}}$ it becomes

$$P^p_{\text{in}} = \frac{P^s_{\text{out}}}{\eta_{\text{PC}}}\left(1 - \frac{1}{G}\right). \tag{3.4}$$

This shows that for large amplification, the pump power has only a weak dependence on the gain. Instead, it is directly proportional to the output power of the EDFA.

3.1.2 The two-level model

To further understand in which cases we can use the added-power model from the previous section, we will study the commonly used two-level model, which was introduced by Saleh et al. in 1990 [41]. The two-level model, as its name implies, models the EDFA system as having two energy levels. Out of the two pump wavelengths mentioned earlier, only the 1480 nm case is an actual two-level, but the model also describes the 980 nm pump system well, even though this pumping scheme involves three energy levels. The reason is that the upper energy level has a much shorter lifetime than the middle one, so at any time the population of the upper level is negligible.

The two-level model relates the input and output powers of any number of pump and signal waves, propagating in either direction in the erbium-doped fiber (EDF). The two-level model is only valid assuming that the gain is not saturated by amplified spontaneous emission (ASE) and ignores the impact of noise power, which can grow to values comparable or even larger than the signal power. However, according to Saleh et al. [41] ASE can be safely neglected for gains less than 20 dB *or* input powers above -20 dBm. Nevertheless, the two-level model can also be extended to include ASE noise [42].

The process of solving the two-level model for one pump wave and one signal wave is described in [43, Ch. 5]. This situation is illustrated in Figure 3.1. With this solution, the pump power can be written as a function of the input and output signal power,

$$P^p_{\text{in}} - P^p_{\text{out}} = \frac{\lambda_s}{\lambda_p}\left(P^s_{\text{out}} - P^s_{\text{in}} + P^s_{\text{IS}}\left(\ln\frac{P^s_{\text{out}}}{P^s_{\text{in}}} + \alpha_s L_{\text{EDF}}\right)\right) \tag{3.5}$$

$$= \frac{\lambda_s}{\lambda_p}\left(P^s_{\text{out}}\left(1 - \frac{1}{G}\right) + P^s_{\text{IS}}\left(\ln G + \alpha_s L_{\text{EDF}}\right)\right). \tag{3.6}$$

Here we have introduced also an output pump power P^p_{out} to account for the pump power not transferred to the signal wavelength or attenuated in the fiber, as well as the attenuation constant α_s and the intrinsic saturation power P^s_{IS}. They are defined as

$$\alpha_s = \rho\Gamma_s\sigma^a_s, \tag{3.7}$$

$$P^s_{\text{IS}} = \frac{Ah\nu_s}{(\sigma^e_s + \sigma^a_s)\tau\Gamma_s}, \tag{3.8}$$

where ρ is the erbium ion density, Γ_s is the signal mode overlap with the erbium ions, σ^a_s and σ^e_s are the absorption and emission cross-sections of erbium at the signal wavelength, A is the cross-sectional area of the beam and τ is the upper-state lifetime. For a typical EDF P^s_{IS} is less than 0.5 mW in the C-band, based on EDF parameters found in [43, Ch. 6].

The two-level model is approximately equivalent to the the added-power model provided that most of the pump power is absorbed in the EDF ($P^p_{\text{out}} << P^p_{\text{in}}$) and and that the signal output power is much larger than the intrinsic saturation power ($P^s_{\text{IS}} << P^s_{\text{out}}$). The first condition can be fulfilled by optimizing the EDF length, which is typically done in a well-designed EDFA, and the second condition is typically fulfilled for a fully loaded wavelength-division multiplexed (WDM) system. In Figure 3.2 the two-level model and the added-power model are compared for two different output powers. The power conversion efficiency in the added-power model

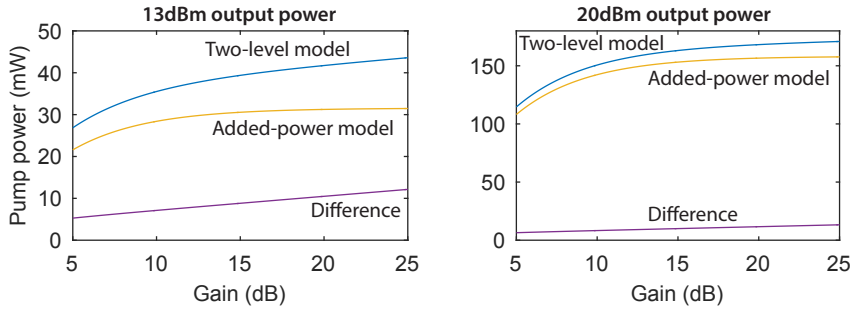

Figure 3.2: Required pump power as a function of gain for the two-level model and the added-power model for two different output powers. Ideal power conversion efficiency is assumed in the added-power model, i.e., $\eta_{\text{PC}} = \lambda_p/\lambda_s$. The pump and signal wavelengths are 980 nm and 1550 nm respectively and the EDF parameters are taken from [43, Ch. 6]. The EDF length is optimized for every gain value.

is assumed to be ideal, i.e., $\eta_{\text{PC}} = \lambda_p/\lambda_s$, which leads the model to underestimate the required pump power.

3.1.3 Amplified spontaneous emission noise

In an EDFA, noise is added to the signal through spontaneous emission. This noise is then amplified by the stimulated emission process, which leads to amplified spontaneous emission (ASE). In a typical system, the ASE does not have any significant impact on the power consumption of the amplifiers, but it has a profound impact on the signal quality. Any noise added to the signal stays and is amplified together with the signal in any subsequent amplifiers, leading to ASE being one of the main transmission-reach-limiting factors. The power spectral density of the ASE can be written [44]

$$S_{\text{ASE}} = n_{\text{sp}} h \nu_0 (G-1), \tag{3.9}$$

where h is the Planck constant, G is the amplifier gain, ν_0 is the frequency of the signal being amplified and n_{sp} is the spontaneous emission factor. The latter is also known as the population-inversion factor, and can be written

$$n_{\text{sp}} = \frac{N_2}{N_2 - N_1} > 1, \tag{3.10}$$

where N_1 and N_2 are the populations of the atomic ground and excited states respectively.

3.2 Distributed Raman amplification

Raman amplification utilizes stimulated Raman scattering to provide optical gain. Its use in modern optical communication systems is mainly due to two important properties that may be advantageous. The first one is that the transmission fiber can be used as the amplification medium, enabling distributed amplification which has beneficial noise properties. The other property is that the absolute spectral position of the gain spectrum is defined by the wavelength of the pump. In silica fiber, the FWHM bandwidth is nearly 6 THz with a peak at 13.2 THz from the pump [45]. Since the pump wavelength determines the position of the gain spectrum, broadband amplification can be achieved by using several different-wavelength pumps.

While the basic concept of Raman amplification is similar to that of EDFAs, i.e., power is transferred from a higher energy pump wave to the signal, distributed Raman amplification is typically operated in a regime widely different from that of EDFAs. Compared to an EDFA, Raman amplification has a low power conversion efficiency, which results in much of the pump power being attenuated in the fiber or remaining at the output of the span.

Distributed Raman amplification can be either backward or forward pumped, or a combination of the two. The pumping schemes determine the evolution of the signal power as well as the noise properties. Since the signal power is maintained at a higher level, forward pumping has better noise properties than backward pumping. However, it suffers worse from other impairments such as pump noise transfer and nonlinear transmission impairments [46]. In addition, Raman amplification is also commonly combined with lumped EDFAs, so called hybrid amplification.

In general, Raman amplification can be described by a set of coupled differential equations that needs to be solved numerically [47]. However, if the signal power is much smaller than the pump power, the normalized signal power evolution is

$$\Gamma(z) = \frac{P_s(z)}{P_s(0)} = \exp\left(g_R \int_0^z P_p(\zeta) d\zeta - \alpha_s z\right), \tag{3.11}$$

where $P_s(z)$ and $P_p(z)$ are the signal and pump power evolutions along the fiber and g_R is the Raman gain coefficient, which is related to the cross section of spontaneous Raman scattering. For a span length of L the pump power evolution is $P_p^{\text{in}}(z) = \exp(-\alpha_p z)$ for forward pumping and $P_p^{\text{in}}(z) = \exp(-\alpha_p(L-z))$ for backward pumping. In the above equations, α_s and α_p are the signal and pump attenuation factors respectively.

The total Raman gain is conveniently expressed as the *on-off gain*, which is the ratio of the signal power at the output of the span with the Raman pump turned on

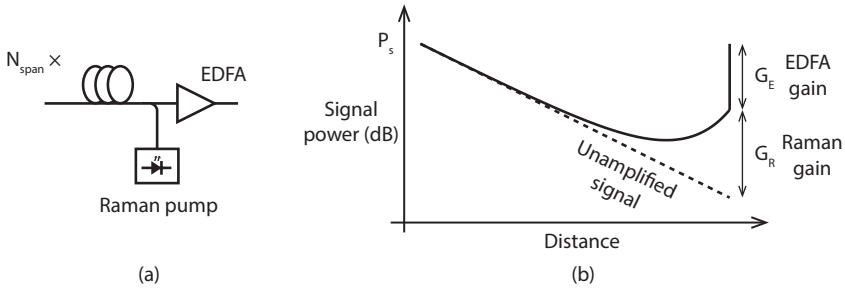

Figure 3.3: (a) Basic schematic of backwards-pumped hybrid EDFA/Raman amplification (b) The signal power evolution along the span for the system in (a).

and the signal power without Raman gain. The on-off gain can be written

$$G_R = \Gamma(L)e^{\alpha_s L} = \exp(g_R P_p(0) L_{\text{eff}}), \tag{3.12}$$

where

$$L_{\text{eff}} = \frac{1 - e^{-\alpha_p L}}{\alpha_p} \tag{3.13}$$

is the Raman effective length. Thus, the pump power has a logarithmic dependence on the gain.

3.2.1 ASE noise and nonlinear effects in Raman systems

The ASE at the output of a Raman amplified span is described by

$$S_{\text{ASE,R}} = n_{\text{sp,R}} h\nu_0 g_R \Gamma(L) \int_0^L \frac{P_p(z)}{\Gamma(z)} dz, \tag{3.14}$$

where $n_{\text{sp,R}}$ is the Raman spontaneous emission factor which among other things depend on the temperature and the Raman shift. For a typical SMF at room temperature $n_{\text{sp,R}} = 1.13$ in the C-band [47, p. 50].

Distributed Raman amplification is often used together with EDFA-based lumped amplification to improve the optical signal-to-noise ratio (OSNR) and handle long spans. For backwards pumped Raman, since the amplification takes place mostly in the end of the fiber span, the reduction of noise power is almost independent of span length. This means that the OSNR improvement due to Raman amplification mostly depends on the Raman pump power. This is further discussed in [Paper A].

The Gaussian-noise (GN) model for non-linear interference described in Section 2.2.3 has been extended to cover also Raman amplified systems [48]. In the general case the signal power evolution needs to be integrated over the whole span, which is not always trivial. However, by approximating the signal power evolution with simple exponential functions it becomes easier [49]. In fact, for backwards pumped hybrid Raman, the effect of the changed power evolution can be neglected for lower Raman gains, and S_{NLI} can be calculated as for a system without distributed amplification. Pelouch [49] states that this is acceptable if the output power from the span is more than 13 dB below the maximum power within the span, and Curri et al. [46] defines this region as when Raman amplification contributes with less than 60% of the total gain in dB.

3.3 Power consumption model

Generally, pump laser diodes are used for both EDFAs and Raman amplification. The power consumption P_p^e can be modeled as being linearly dependent on the optical power P_p^o input to the fiber

$$P_p^e = \frac{1}{\eta} P_p^o, \tag{3.15}$$

where η is a power conversion efficiency that include all sources of inefficiencies that are proportional to the pump power. Here we have introduced the superscripts e and o to distinguish between electrical power and optical power.

The factor η includes several sources of inefficiencies. Firstly, the coupling of pump power into the amplification fiber has a limited efficiency. Secondly, the pump laser has some electrical-to-optical power conversion efficiency and thirdly, diode lasers in many cases require active cooling with thermoelectric coolers (TECs) to maintain wavelength stability, whose power consumption can be included in an efficiency factor.

To find the conversion efficiency η, we start by writing the power consumption as the sum of the power consumption of the laser diode and the TEC

$$P_p^e = P_{\mathrm{LD}}^e + P_{\mathrm{TEC}}^e, \tag{3.16}$$

where the power consumption of the laser diode is proportional to the optical output power, $P_{\mathrm{LD}}^e = P_{\mathrm{LD}}^o/\eta_{\mathrm{LD}}$, and the power consumption of the TEC is proportional to the heat removed Q_{LD}, so that $P_{\mathrm{TEC}}^e = Q_{\mathrm{LD}}/k_{\mathrm{TEC}}$. Here k_{TEC} is the TEC coefficient of performance (COP) [50]. The heat removed with the TEC can be assumed to be equal to the electrical power not converted to optical power in the laser diode

and thus found by subtracting the optical output power from the laser diode power consumption, so

$$P^e_{\mathrm{TEC}} = \frac{1}{k_{\mathrm{TEC}}}(P^e_{\mathrm{LD}} - P^o_{\mathrm{LD}}) = \frac{1}{k_{\mathrm{TEC}}}\left(\frac{1}{\eta_{\mathrm{LD}}} - 1\right) P^o_{\mathrm{LD}}. \tag{3.17}$$

This leads to the the total power consumption

$$P^e_{\mathrm{pump}} = \left(\frac{1}{\eta_{\mathrm{LD}}} + \frac{1}{k_{\mathrm{TEC}}\eta_{\mathrm{LD}}} - \frac{1}{k_{\mathrm{TEC}}}\right) P^o_{\mathrm{LD}} \tag{3.18}$$

which is proportional to the optical output power. To include also the coupling into the amplification fiber we can replace the laser diode output power with the pump power needed in the amplification fiber

$$P^e_{\mathrm{pump}} = \frac{1}{\eta_c}\left(\frac{1}{\eta_{\mathrm{LD}}} + \frac{1}{k_{\mathrm{TEC}}\eta_{\mathrm{LD}}} - \frac{1}{k_{\mathrm{TEC}}}\right) P^o_{\mathrm{pump}}, \tag{3.19}$$

where η_c is the coupling efficiency.

The TEC COP depends on the temperature difference between the hot and the cold side of the TEC. For low temperature differences it can be above 100%. However, the temperature in equipment huts can be as high as 75°C while the laser diode should be kept at 25°C. In this worst case temperature difference of 50 K, the typical COP is only 17% [51]. Although Raman pump laser diodes can have a power conversion efficiency of 25% [52], when this is combined with the other inefficiencies and input into Eq. (3.19) an overall electrical to coupled pump power efficiency of 3% is found. Here, a coupling efficiency of 1.5 dB was assumed. EDFA pump lasers can have a higher efficiency since they do not necessarily require active cooling (e.g. [53]). For example, in [54] an overall electrical to signal power conversion efficiency of 5% was used. This included also the power conversion between pump and signal.

In addition to the power consumption of the pump lasers, which is directly related to the operating conditions of the amplifier, such as output power and gain, optical amplifiers also include control and management circuitry that consumes power. This power consumption, which will be referred to as the *monitoring and management* can be modelled as being independent of the operating conditions of the amplifier, i.e., a constant term added for each amplifier unit. If just one amplifier is studied the value of the monitoring and management power consumption does not affect the optimum point, but in a system optimization scenario where the number of amplifiers is allowed to vary it may affect the optimum point significantly.

Choosing a value for the monitoring an management power consumption presents a challenge as estimates varies widely between different sources. In [9] a value as

high as 100 W is used for the total EDFA power consumption and [20] uses a value of 55 W for the monitoring and management power consumption. In [55, 56] the whole amplifier power consumption is estimated to be between 30 W and 60 W. In contrast to these values, Desbruslais et al. [54] use a value of 10% of the total amplifier power consumption, which would correspond to sub-Watt values for a typical amplifier.

3.4 System optimization

By combining power consumption and noise models, the relation between system performance and amplifier power consumption can be studied. Several studies of this has been published and depending on the exact system model used the results may differ. In this section the different approaches and results are compared and discussed.

3.4.1 EDFA

One of the simplest system models is to combine the added-power model with the standard OSNR model. In [9] this is done to estimate the theoretical lower limit on amplifier power consumption. In this model, the power consumption is directly proportional to the signal launch power, and fiber nonlinearities are neglected. If the required SNR is fixed, the power consumption becomes directly proportional to the noise power added in the line amplifiers. Thus, the power consumption grows exponentially with system length. Shorter spans lead to a slower build-up of ASE noise, and thus result in a lower power consumption. The span length that achieves the lowest power consumption is zero, which corresponds to ideal distributed amplification.

The situation changes if nonlinear effects are considered. Doran and Ellis [57] investigate the situation where performance is determined by the GN-model and optical output power is used as a power consumption measure. Then, the power consumption can be analyzed analytically, and an optimum point that minimizes the power consumption can found. Depending on how the signal launch power is chosen the optimum point will be different. Either, the system can be operated at the nonlinear threshold (in this thesis Eq. (2.4)), or the signal power can be chosen to always achieve a certain OSNR. In the first case, where the system is operated at the nonlinear threshold the span length that gives the minimum power consumption is $L = 3/\alpha$, where α is the fiber attenuation in m^{-1}. This corresponds to a loss of 13 dB, which for a typical SMF is 65 km. In the second case, which is a more global optimum, the span length is shorter than in the first case. The minimum points exist due to the following trade-off: For span lengths longer than the optimum, the power consumption increases since the increased ASE requires the signal launch power to be increased.

For span lengths lower than the optimum, the power consumption increases since more EDFAs are needed.

In [Paper A] we investigate the system level power consumption by combining the added-power model (including the monitoring and management power consumption) with the GN-model. In a multi-span system, if the system is assumed to be operated at the optimal signal launch power the power consumption can be studied as a function of the OSNR by varying the number of spans, and thus the span length. When the number of spans is increased, the OSNR is increased. Since the amount of ASE then is lower, the optimal signal launch power is also lower. This leads to the pump power consumption being lower. However, since the number of amplifiers is increased the total monitoring and management power consumption is increased. This means that for a fixed system length, the OSNR that gives the lowest amplifier power consumption will be a trade-off between pump power consumption and monitoring and management power consumption.

3.4.2 Hybrid Raman amplification

Due to its low power conversion efficiency, distributed Raman amplification generally requires significantly higher pump power to provide the same gain as an EDFA. However, its beneficial noise properties can lead to power savings in other parts of the systems that outweigh the increased pump power consumption [Paper A]. These situations are either if the monitoring and management power consumption is high or if the OSNR requirement is high, such as for high-order modulation formats.

Chapter 4

Digital signal processing

One of the key factors to the success of coherent detection is that the access to the full optical field enables the use of digital signal processing (DSP) to be used to efficiently compensate linear transmission impairments. In addition, DSP enables the use of a free-running local oscillator (LO), since frequency offset and phase noise can be tracked digitally, which avoids the use of complex analog control loops. However, the digital circuits performing the processing is one of the major power consumers in a coherent receiver [20].

In this chapter we cover the basics of digital signal processing in coherent fiber-optical communication systems, along with an overview of implementation and power-consumption issues.

4.1 Overview of DSP for coherent systems

Coherent optical communication relies on digital signal processing in several steps. In Figure 4.1, a schematic of a typical DSP-chain is shown. Signal processing is needed both to compensate for impairments caused by non-ideal components and fiber-related transmission impairments.

4.1.1 Optical front-end correction

Optical front-end correction compensates for the impairments introduced by the photodetectors and the optical hybrid. This is done in two steps: Normalization and orthogonalization. Normalization is performed separately on each of the quadrature signals to make sure that they have the same average power, which compensates for

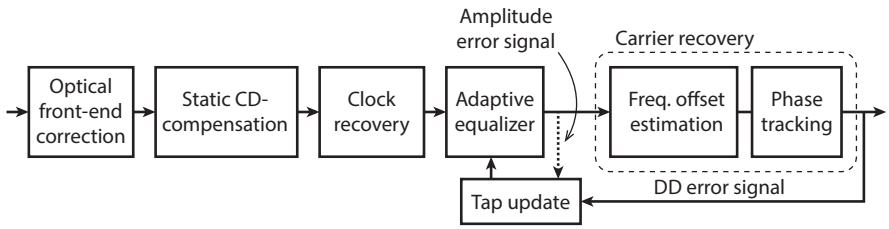

Figure 4.1: A typical DSP-chain. The adaptive equalizer can either take amplitude or decision-directed error information for the tap update. In the latter case, the error needs to be calculated after the carrier recovery stage.

unequal responsivities of the photodetectors. Orthogonalization removes any linear dependence between the quadratures, which can be cause by an imperfect 90° phase-shift in the optical hybrid. The most common orthogonalization algorithm is the Gram-Schmidt process [58], but as it distributes the quantization noise unevenly, other methods such as the Löwdin algorithm might be beneficial [25]. Similar methods can be used also after the DSP chain to compensate for a non-optimal modulator bias-point.

4.1.2 Chromatic dispersion

Chromatic dispersion (CD) is commonly compensated in a static filter. It can be performed by an FIR filter in time or frequency domain. The filter taps can be found by directly sampling and truncating the continuous CD compensation filter impulse response [59], but if the taps are finite precision, there will be a penalty due to quantization errors. This penalty can be minimized by optimizing the tap values [60]. For long-haul systems, where large amounts of dispersion needs to be compensated for, it is more hardware efficient to implement dispersion compensation filters in the frequency domain [25], but for link lengths below 150 km, time domain filters are more efficient [61].

4.1.3 Clock recovery

Clock recovery can be divided into two parts. The first is synchronization of the clock *frequency*, i.e. the exact time base used by the transmitter to determine the symbol rate. The other is recovery of the right *sampling phase* or *symbol timing*, which equivalent to determining the optimal time instant to sample in the middle of the signal. To avoid confusion we will use the terms *clock frequency recovery* for the

first and *timing recovery* for the latter. While timing recovery is always necessary, the need for clock recovery depends on the transport protocol used. SONET/SDH are synchronous standards where clocks are synchronized over the system, while Ethernet allows the clocks to differ, and thus requires clock frequency recovery.

Several algorithms exist for performing timing recovery separately [25], but it can also be performed by adaptive finite impulse response (FIR) filters [62] like those needed for compensation of polarization-mode dispersion (PMD), discussed in next section.

4.1.4 Adaptive equalization

Adaptive equalization is needed to compensate for time-varying effects. In a fiber-optic system the most important time-varying effects are polarization changes and PMD. Since polarization rotations causes linear mixing of the two polarizations, polarization demultiplexing is performed with a 2×2 multiple-input multiple-output (MIMO) equalizer. For this, only one filter tap is needed. However, since PMD introduces frequency dependent cross-talk between the polarizations, more taps are needed.

In addition to the time-varying effects, due to the adaptivity of the filter, the taps will adjust to compensate also static linear impairments remaining on the signal. This includes any CD not compensated for by the static CD equalizer and filtering characteristics in the signal paths, such as digital-to-analog converters (DACs), modulator, photodetectors and analog-to-digital converters (ADCs). The filter will also converge to match the signal spectrum, acting as a matched filter providing optimal noise filtering. If the error function used in the tap updating is sensitive to phase errors, slow phase variations can also be tracked. It is also common to perform downsampling in the adaptive equalizer in which case it will act as a timing recovery stage.

For QPSK the constant-modulus algorithm (CMA) [63, 64] is commonly used for tap update [25], relying on the constant power of the QPSK symbols. While it still works for higher order modulation formats, the tap updates become noisy which leads to poorer performance [25]. The CMA can be modified for higher order modulation formats to include several power levels, known as radius-directed equalization (RDE) or the multi-modulus algorithm (MMA) [65–68]. However, for modulation formats with many radius levels such as 64QAM, this performs poorly. Another option is to use decision-directed (DD) update, where the error is the distance to the closest constellation point [65, 68]. This has the added advantage of being sensitive to phase, which means that the equalizer can track slow phase variations. However, this means that the error calculation needs to be done after the carrier recovery stage, which then ends up inside of the equalizer update loop.

4.2 Carrier recovery

DSP-based carrier recovery is commonly divided into steps, where a first coarse carrier recovery compensates for the main parts of the frequency offset. Once this offset has been removed, significant amounts of phase noise remain on the signal, which is estimated and compensated for by the phase-tracking.

4.2.1 Frequency offset estimation

The frequency offset can be estimated by finding the peak of the spectrum of the 4th power of the signal [25], which relies on the same principle to remove the modulation as the Viterbi-Viterbi algorithm [69] described later. Although the modulation cannot be completely removed for higher order QAM formats, this method is still useful, albeit with a lower accuracy.

4.2.2 Feedback-based phase-tracking

Early coherent receivers were based on analog phase-locked loops for carrier recovery [70], where an error signal calculated from the signal is used to tune the frequency of the LO laser. The feedback principle can also be used in DSP, for example as in the DD phase estimator in [71]. In this algorithm, the signal is derotated with the phase angle estimated from a previous symbol, with some feedback delay. This algorithm can achieve high tracking speeds if the feedback delay is low. However, the effect of the parallelization necessary in an ASIC implementation is to increase the delay, so the tracking speed is severely limited in a hardware implementation [72]. Still, feedback methods can be used if they are combined with faster algorithms [73].

4.2.3 The Viterbi-Viterbi algorithm

For QPSK, the Viterbi-Viterbi algorithm [69] is commonly used. Single amplitude M-PSK modulation formats has the property that if the M-th power of the symbols is taken, all symbols are mapped to the same point. This has the effect of removing the modulation, and can be used to estimate the phase variations [25]. For QPSK, $M = 4$, and the estimated phase is

$$\phi_k = \frac{1}{4} \sum_{|n|<L/2} w_n \arg\left[Z_{k+n}^4\right], \tag{4.1}$$

Here Z_k is the k-th symbol. To minimize the effect of additive Gaussian noise, estimates of a block of consecutive symbols are weighed together with the weigthing function w_n. In the simplest case, all $w_n = 1$ which is just a sliding average.

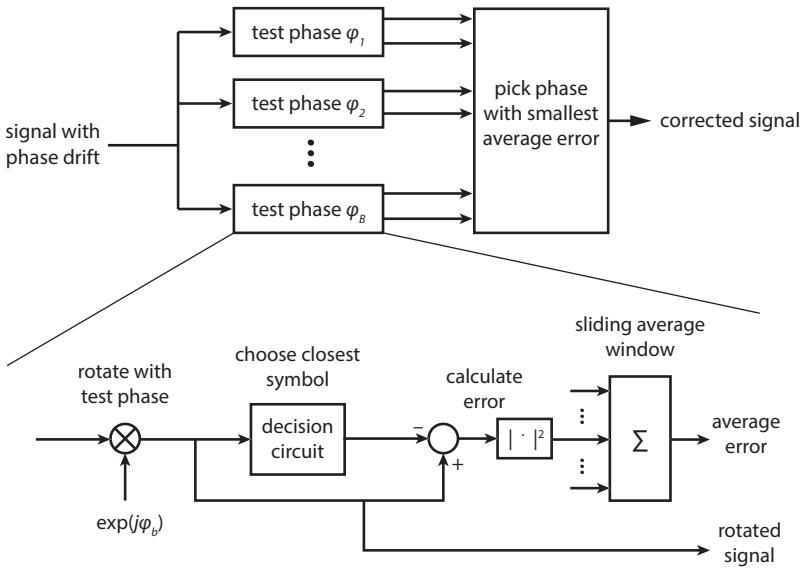

Figure 4.2: Schematic of the BPS algorithm.

Since higher order QAM formats do not fulfill the single-amplitude condition, the Viterbi-Viterbi algorithm does not work well. However, this can be overcome by partitioning the symbols into groups with constant amplitude and applying the Viterbi-Viterbi algorithm to these [74].

4.2.4 Blind phase search

The blind phase-search (BPS) algorithm was first proposed in [75] and introduced to fiber optical communication in [72]. The working principle is as follows. The received signal Z_k, sampled at symbol rate, is first rotated with B test phase angles simultaneously

$$\phi_b = \frac{b}{B} \cdot \frac{\pi}{2}, \quad b = 0, 1, ..., B-1 \tag{4.2}$$

after which the distance to the closest constellation symbol is calculated for each test angle as

$$|d_{k,b}|^2 = |Z_k e^{-j\phi_b} - \hat{X}_{k,b}|^2. \tag{4.3}$$

To reduce the impact of additive noise, the distances are then summed for L consecutive symbols

$$e_{k,b} = \sum_{|n|<L/2} |d_{k-n,b}|^2, \tag{4.4}$$

and the estimated phase angle is chosen as the one that minimizes $e_{k,b}$. The length of the summing window L is chosen as a trade-off between additive noise tolerance and phase-noise tolerance, where a higher tolerance to phase noise is achieved for large values of L. The strength of the BPS algorithm is that it can achieve high tracking speeds even if it is parallelized. This is because the BPS algorithm is inherently parallel as all test angles are calculated simultaneously. However, even if it was introduced to fiber optics as being "hardware efficient" the computational load scales linearly with the number of test angles. Thus for higher order QAM formats such as 64QAM that require a high angular resolution, the hardware requirements of BPS might become prohibitively high [76].

To address this and other issues, several variations and extensions of the BPS algorithm have been proposed. The phase estimation can be divided into several stages [76], where a first stage providing a coarse estimate is followed by a more precise second stage. The different stages can use different algorithms [76, 77] or both be of the BPS type [78, 79]. One approach relies on the fact that $e_{k,b}$ can be approximated as a quadratic function of the test angle ϕ_b, independently described in [80] and [81]. By applying a correction angle $\phi_{k,c}$ calculated using a quadratic approximation of $e_{k,b}$, the number of test angles needed can be significantly reduced. The final estimated phase angle is then

$$\phi_k = \phi_{k,b} + \phi_{k,c} = \phi_{k,b} + \frac{\Delta\phi}{2} \cdot \frac{e_{k,b-1} - e_{k,b+1}}{e_{k,b-1} + e_{k,b+1}}, \tag{4.5}$$

where $\Delta\phi = \pi/(2B)$ is the spacing between the test phase angles. The phase tracking in [Paper C] was based on this method.

4.2.5 Phase unwrapping and cycle slips

All the blind phase estimation algorithms discussed have a limited estimation range, and thus require phase unwrapping. The Viterbi-Viterbi algorithm produces phase values between $-\pi/M$ and $-\pi/M$ and the DD feedback algorithm is constrained to output values between $-\pi$ and π [71]. The output range of the BPS algorithm depends on the symmetries of the modulation format used. For square QAM, the output of BPS is constrained to a $\pi/2$ range. When the phase reaches the end of the estimation range, the estimated phase will wrap around and make a jump to the other end of the range. This jump can be detected, and the phase unwrapped by

adding an integer multiple of the estimation range. However, if the phase jump was present in the actual phase, phase unwrapping will cause a persistent phase error of a multiple of $\pi/2$. This is known as a *cycle slip*, which leads to catastrophic failures. To mitigate the effect of cycle slips, differential encoding can be used. Then, for square QAM, the two bits that determine the quadrant is differentially encoded similar to differentially encoded QPSK [71, 72]. However, this leads to an SNR penalty. Differential encoding is studied in detail in [82].

4.3 Nonlinearity compensation

Compensation of nonlinear effects is highly desirable as they are a main limiting factor for fiber optical communication systems, and many methods have been proposed to mitigate this impairment [83]. However, they are not widely employed in commercial systems, likely due the computational complexity of many of the algorithms.

Maybe the most popular method is *digital back-propagation* [84] (DBP), which can be described as inputting the received signal to a simulated backwards system with opposite signs on the coefficients for dispersion, nonlinearities, and loss. This is typically performed with the split-step Fourier method, which is computationally intensive due to the need to perform multiple Fourier transform operations repeatedly while stepping through the fiber [85]. Fundamentally, DBP is limited by stochastic processes such as PMD and ASE, as well as nonlinear effects involving these [86, 87]. Furthermore, DBP can only undo nonlinear interaction involving the signal bandwidth available in the receiver. If only a single channel is received, no compensation of inter-channel interactions can be performed [88]. Nevertheless, using wide bandwidth receivers, multi-channel DBP has been demonstrated [89, 90]. In multichannel DBP, a further limiting factor is the uncertainty in the relative spectral positions of the channels, caused by the frequency drift of the carrier lasers. This effect can be avoided by taking the carriers from a frequency comb instead [91].

Despite its computational complexity, DBP can be implemented in hardware for single channel [85, 92] with reasonable power consumption [93]. However, the implementation of multichannel DBP remains to be demonstrated.

As discussed in Section 2.2.3, inter-channel nonlinear interference partly manifests itself as phase and polarization rotation noise (PPRN) which has correlation times long enough to allow it to be tracked by a fast MIMO equalizer [32, 94]. One method for increase the update speed of such an equalizer is to use of 4D modulation formats deigned to minimize the number of symbol errors [95, 96]. However, implementing such an equalizer in real-time in hardware would likely be challenging, due to the need for parallelization in which limits the update speed of feedback structures [72].

4.4 Implementation and power-consumption aspects

Due to the high throughput requirements, DSP for optical communication is generally implemented as application specific integrated circuits (ASICs). Implementation of real-time DSP presents several challenges.

Parallelization

As the typical clock frequency of an ASIC is below 1 GHz, it is not possible to process optical signals in a serial manner. Instead, parallelization is used, which means that the signal and subsequently all processing units are divided into several parallel data streams and processing blocks. For many DSP functions this can be readily done without impacting the performance, but it might limit the tracking speed of fast time-varying impairments such as phase noise.

Quantization

Floating point arithmetics leads to a too high circuit complexity to be implemented in optical DSP. Therefore, computations are performed using fixed-point arithmetics which requires quantization of the signal. Since complexity and power dissipation increases with the number of quantization levels, it is desirable to use as few quantization levels as possible without giving rise to a penalty due to quantization noise. Generally, higher order modulation formats require more quantization levels.

4.4.1 Power consumption

The power consumption of ASICs depends on the logic functions they perform and the clock-frequency of which the circuit runs in a complex manner. This is because fundamentally the power consumption is determined by the physical layout of the circuit on a transistor level, where also internal interconnecting wires may play a significant role. In addition, the power consumption depends on the signal being processed [97, Ch. 5]. This makes it hard to estimate power consumption directly from any given algorithm. As of today, the most reliable way of estimating the power consumption of a DSP algorithm is to design an ASIC—including physical layout—and simulate it with realistic input signals. Since this requires considerable ASIC-design skills and then a significant workload, analysis of algorithms tend to be based on computational complexity, where the number of operations required for an algorithm is compared. While this is often the only feasible option, the results can only give a rough indication of actual power consumption [98].

An alternative is scaling values from an ASIC implementation with some design parameter, as in [Paper B] where we used the equalizer design in [98] and rescaled with the number of taps. This was possible since the equalizer considered in [Paper B] have a similar structure to the one in [98].

4.4.2 Relative power consumption of the steps in DSP for optical communications

In [20], Pillai et al. analyze DSP power consumption by basing their estimates on counting operations, while Crivelli et al. [73] and Morero et al. [27] base their values on actual power consumption of commercial chips. Although the individual estimates differ, the overall picture is similar. All three sources find that compensation of chromatic dispersion is the major power consumer followed by the adaptive equalizer responsible for PMD-compensation. While carrier recovery is found to be on third place, it still has a significantly lower power consumption than the top two. Both [20] and [27] compare QPSK to 16QAM and find that the higher order format achieves an equivalent [20] or lower [27] power consumption per bit.

In a long-haul link, where high amounts of CD and PMD needs to be compensated for, the DSP power consumption is comparable to that of optical components such as lasers, modulators and optical amplifiers [20]. However, in the short-reach limit where no length dependent signal impairments are present, the DSP functions consume only a small part of the power [Paper B].

Chapter 5

Phase-coherent superchannels

A *superchannel* is a set of classical optical channels that is treated as a single entity, i.e. they are transmitted, routed, and received together. The subchannels can be multiplexed either in the *spectral* domain [17] in a single-mode fiber or the *spatial* domain [99] in multicore and mode-multiplexed transmission. Although spectral and spatial superchannels rely on quite different physical principles for multiplexing the subchannels, they share some common characteristics that motivates them to be discussed together. The first characteristic is that in many cases the carriers used for the subchannels are phase-coherent, and the second is that the full superchannel (despite consisting of many channels) is received at one location, which allows the subchannels to be processed together. In this chapter, we discuss *phase-coherent* superchannels (illustrated in Figure 5.1), based on either optical frequency combs, or spatial division multiplexed (SDM) systems using a shared carrier. We describe the properties of optical frequency combs as well as how the phase coherence of the superchannel is affected by transmission.

5.1 Frequency combs and spectral superchannels

An optical frequency comb is a light source whose spectrum consists of a set of evenly spaced, narrow spectral lines that are phase-locked to each other. In addition to optical communications, frequency combs have many applications, including high precision time-keeping [100], spectroscopy [101], range measurements [102, 103] and signal synthesis [104, 105]. Also before the concept of superchannels was introduced, frequency combs were considered for use in optical communication [106, 107]. The first demonstrations were performed with on-off keying modulation [108–

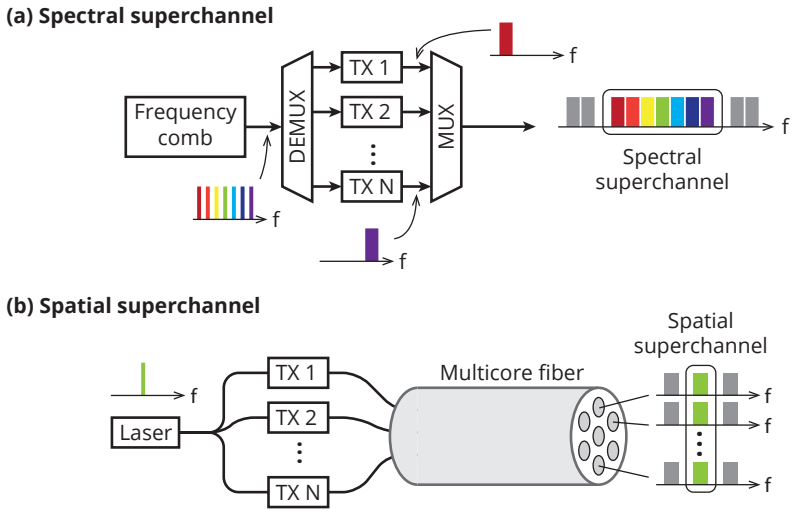

Figure 5.1: Illustration of the two superchannel concepts.

111], and used a frequency comb for its ability to replace hundreds of separate lasers.

With the advent of optical OFDM, the frequency stability of the lines made optical frequency combs attractive, as a stable spacing between the optical carriers is crucial to create a seamless, broadband optical OFDM signal [17]. Optical frequency combs also allow for all-optical OFDM, where no intermediate step of electrical OFDM signals is required [112]. Also for standard wavelength-division multiplexed (WDM) transmission the frequency stability of optical frequency combs offer advantages. A spectral superchannel based on WDM subchannels can in principle use carriers originating from multiple independent lasers. However, the frequency drift of lasers requires guardbands between the channels of at least a couple of GHz, which represents an unacceptable loss of spectral efficiency in many applications. Furthermore, the frequency stability can improve the efficiency of compensation of nonlinear effects [91].

There are many methods for generating optical frequency combs. The first demonstration widely recognized as a frequency comb used the electro-optical modulation technique [113, 114], which since has been developed into many different variations. Due to their flexibility and high performance [115], they are a good choice for WDM transmission [116]. Also mode-locked lasers can be used for optical communication [117, 118], including OFDM [112] and other coherent formats [119, 120].

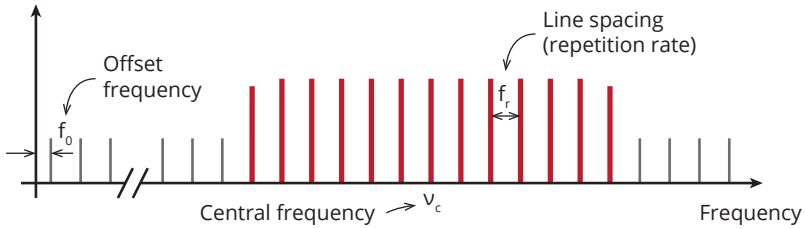

Figure 5.2: Frequency comb definitions.

A third category is parametric combs that are generated by four-wave mixing (FWM) in a nonlinear medium [121]. This technique starts from two carriers (ideally phase locked to each other), whose frequency difference determines the overall line spacing of the resulting comb. Another alternative is to launch a full frequency comb generated through some another technique into the nonlinear medium, which is then broadened by FWM. In this way frequency combs spanning a full octave can be generated, which is important for applications requiring an absolute frequency reference [104, 122]. For telecommunication, the potential for parametric broadening is instead that a single comb source can cover the full C- and L-bands [123, 124].

In many applications, the physical size of the device creating the frequency comb is important. Both electro-optical frequency combs [125, 126] and mode-locked lasers [127] have been demonstrated on chip-scale. In integrated platforms frequency combs based on microresonators are possible [128], and have been demonstrated for optical communication [129–133], also for high spectral-efficiency systems [134].

5.1.1 Phase and frequency relations

The positions of the lines of an ideal frequency comb can be described by only two parameters according to

$$f_k = kf_r + f_0, \quad k = 0, 1, 2, ..., \tag{5.1}$$

where f_r is the spacing between the spectral lines and f_0 denotes the offset from zero. This means that the the absolute frequencies of the comb lines are not necessarily multiples of f_r. In the time domain, a frequency comb is a train of pulses with repetition rate f_r. The quantity f_0 then describes the shift of the carrier-envelope offset between each pulse, i.e., the phase difference between the optical carrier wave and the pulse envelope.

For a slightly less ideal frequency comb, i.e., one that does not span the full range

of frequencies from zero and up to optical frequencies, a useful notation is

$$f_n = \nu_c + n f_r \quad n = 0, \pm 1, \pm 2, ..., \tag{5.2}$$

where ν_c is the center frequency of the comb. This is particularly natural for combs that are generated by modulation of a continuous wave (CW) tone, as the frequency of this tone defines ν_c. It is also commonly used in telecom applications, as it can be assured that the comb lines end up on a standardized frequency grid by setting ν_c to be on the grid and f_r to correspond to the grid spacing.

Introducing more non-idealities, it is useful to instead write the full electric field of the comb,

$$E(t) = \sum_k E_k \exp[-i2\pi(f_k t + \phi(t) + k f_r \Delta T(t))], \tag{5.3}$$

where the complex amplitude E_k and the phase noise terms $\phi(t)$ and $\Delta T(t)$ have been introduced. In this expression, $\phi(t)$ is the phase noise of the carrier frequency, and $\Delta T(t)$ is the timing jitter noise of the pulse train. Using the alternative notation, the same relation can be written

$$E(t) = \sum_n E_n \exp[-i2\pi(f_n t + \phi_0(t) + n\psi(t))]. \tag{5.4}$$

In this expression, $\phi_0(t)$ is the phase noise of the center line and $\psi(t)$ is phase noise that originates from the comb generation process. With this notation, the phase evolution of the nth line can be written

$$\phi_n(t) = \nu_c t + \phi_0(t) + n(f_r t + \psi(t)). \tag{5.5}$$

The importance of this equation is that although frequency combs are described as having phase-coherent lines the coherence is limited by the line dependent phase noise term. The general behavior of the phase relations is general for several different comb technologies, including mode-locked lasers [135, 136], electro-optical frequency combs [137] and nonlinearly broadened combs [121, 138]. However, the origin of the different phase noise terms differs for different technologies. For electro-optical frequency combs, the term $\phi_0(t)$ is the phase noise of the seed laser and $\psi(t)$ corresponds to the phase noise of the radio-frequency (RF) oscillator driving the modulators [137] (which we demonstrated in [Paper D]). Since RF-oscillators can have very good phase noise performance, the function of an electro-optical comb can be seen as simply copying the properties of the seed laser. By choosing a low phase-noise seed laser, a wide comb of low phase-noise lines can be created.

For parametric combs, the line dependent phase noise term depend on the phase noise differences between the two lines used to create the comb [121, 138]. Therefore, the two lines need to be phase-locked to each other for the comb not to suffer from excessive phase noise.

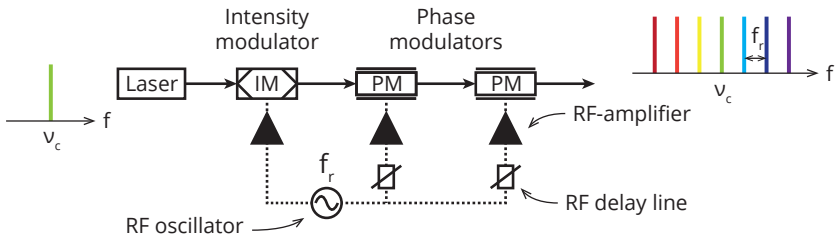

Figure 5.3: A common setup for creating an electro-optical frequency comb.

5.1.2 Electro-optical frequency combs

Electro-optical frequency combs (often referred to as EO-combs) are created by modulating CW light with an RF signal. This creates sidebands around the CW tone spaced by the frequency of the RF signal. Electro-optical frequency combs exist in many varieties [139]. Here we will describe in detail the implementation used in the papers included in this thesis [115]. A CW laser line is fed into one or multiple cascaded electro-optical phase modulators. The phase modulators are driven with a sinusoidal RF-signal. The modulation depth of the phase modulation determines the number of sidebands created, which determines the bandwidth of the produced frequency comb. By using several cascaded phase modulators, the modulation depth can be increased more than the limit posed by the maximum RF power-handling capabilities of one single modulator.

However, the comb resulting from only a sinusoidal phase modulation has large power variation between the lines. One method to equalize the power is to use an intensity modulator cascaded with the phase modulators. The intensity modulator is biased to produce close to square pulses, that are aligned in time with the linear part of the chirp induced by the phase modulators. The process can be understood in terms of the space-time analogy, where the phase modulation represents a time lens [140], which causes the spectrum to take the same shape as the pulses produced by the intensity modulator [141]. With this setup combs with a spectral power variation below 6 dB can be created. Although flatter electro-optic combs can be created by driving the modulators with more complex RF waveforms [141], the above implementation is a good trade-off between complexity and performance.

The power consumption of electro-optical comb generation can be quite high if broadband phase modulators with high V_π are used. However, using electrodes resonant at the modulation frequency, the V_π can be reduced [142], potentially leading to more power efficient comb generation.

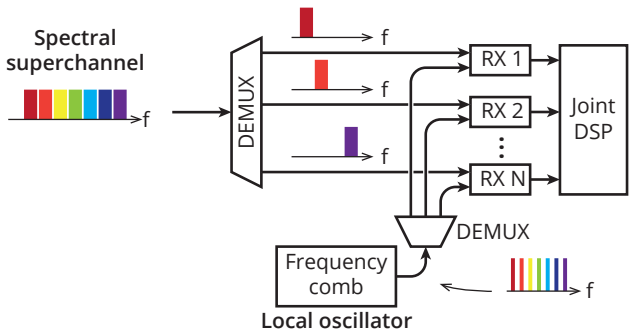

Figure 5.4: Schematic of a frequency-comb based receiver with joint DSP.

5.1.3 Frequency-comb based receivers

To be able to take advantage of the phase coherence of the channels in the receiver, the phase coherence needs to be preserved after detection. Since the local oscillator (LO) also contributes to the phase noise, this essentially means that the LOs also needs to be phase-coherent. One alternative to achieve this is to detect many channels in a single coherent receiver using a single LO line, as in [143, 144]. However, this method will limit the superchannel bandwidth to the detector bandwidth. More scalable is instead to use several coherent receivers, using lines from a frequency comb as LOs, as illustrated in Figure 5.4. In the following description, we will assume that each coherent receiver will receive a single subchannel, but it should be noted that with some additional DSP this setup can be used as a single, broadband receiver through spectral slicing [89, 145].

The phase noise of the detected channels can be written

$$\begin{aligned}\phi_n(t) = 2\pi(\nu_{0,S} - \nu_{0,LO})t + (\phi_{0,S}(t) - \phi_{0,LO}(t)) + \\ + n(2\pi(f_S - f_{LO})t + \psi_S(t) - \psi_{LO}(t)),\end{aligned} \tag{5.6}$$

where the same notation as Equation (5.5) is used, with the additional subscripts S and LO denoting the signal and LO contributions respectively. This equation is general for all comb-based superchannel systems, and it is useful to consider some special cases. One is that when the transmitter and receiver comb have the same spacing ($f_S = f_{LO}$) and the line dependent phase noise is negligible ($\psi_{S,LO}(t) \approx 0$), all received channels share the same carrier offset and phase noise, which is the basic assumption for joint carrier recovery in its simplest case. If this assumption does not hold, the fact that a frequency comb can be described by only two parameters

means that the phase evolution of any channel k can be calculated from two arbitrary channels m and n as

$$\phi_k(t) = \phi_n(t) + \frac{k-n}{m-n}[\phi_m(t) - \phi_n(t)]. \tag{5.7}$$

So far, a joint carrier recovery scheme using this relation has not been experimentally demonstrated, but the relation is very well illustrated by the measurements we presented in [Paper D].

Furthermore, assuming that the line-dependent phase noise is negligible, but the spacing difference of the signal and LO comb is not ($f_S \neq f_{LO}$), the detected channels will be affected by the same phase noise but have different frequency offsets. This was the case in [Paper F], where we also showed that the spacing difference could be extracted from two received channels.

Another special case is when the LO comb has *exactly the same* center frequency and phase noise as the transmitter comb. This occurs in frequency-comb-based *self-homodyne* systems (self-homodyne systems in general are discussed in Section 6.2), where the LO comb has been phase-locked to the transmitter comb. Then the frequency offset and phase noise of the channels is cancelled out by the mixing in the coherent receiver, and ideally no digital carrier recovery is needed. Locking the LO comb to the transmitter comb has been demonstrated by leaving two comb lines unmodulated and using them as pilot tones, relying on the relation in Eq. (5.7) to recreate the phases of the full transmitter comb [138, 146–148]. By transmitting a single pilot tone, the bulk of the frequency offset and phase noise is removed [149]. We also discuss the different schemes in [Paper C].

5.2 Spatial superchannels

The main motivation behind SDM is to add a further dimension to scale into, to be able to increase the throughput of a single fiber [18, 150]. In fact, the full bandwidth of a lone SMF has been predicted to soon limit the throughput of optical transmission systems, sometimes referred to as the "capacity crunch" [151]. Indeed, SDM has enabled several transmission records [152, 153].

There are two main types of SDM systems, relying on different types of fiber. Either the fiber can be fabricated with multiple cores, or to support several spatial modes in single core. Multicore fiber was first proposed for communication purposes in 1979 [154], and mode-multiplexing was demonstrated in the beginning of the 80's [155]. It is also possible to combine the concepts through multicore-multimode fiber [152], where each core supports multiple spatial modes, or coupled core fiber

where the cores are placed close together and couple strongly [156], which behaves similar to a multimode fiber.

One of the proposed advantages associated with SDM systems is that the spatial channels can share some system components, such as optical amplifiers [157] and carrier and LO sources. Apart from being beneficial from an integration and power consumption perspective, the latter means that the spatial channels will be affected by the same phase noise. The phase coherence is then maintained during transmission due to the stable phase relation between the spatial modes owing to them sharing the same physical environment in the fiber [99, 158, 159].

5.3 Impact of transmission on phase coherence

The impact of transmission on the phase coherence of both spectral and spatial superchannels can be divided into static time delays and nonlinear effects. We will discuss them separately below.

5.3.1 Dispersion and skew

For spectral superchannels, the chromatic dispersion of the fiber will cause a walk-off between the different wavelength sub-channels, unless broadband optical dispersion compensation is used. While this effect will not be present for spatial superchannels using the same wavelength, other fiber properties cause similar walk-off. In multicore fibers, imperfections in the manufacturing process causes the cores to have slightly different refractive index, which causes an inter-core temporal skew. This skew is on the order of 100 ps/km [160]. Also in mode-multiplexed systems, differential group delay between modes will cause a time-skew.

5.3.2 Nonlinear phase noise

As discussed in Section 2.2.3, nonlinear interference constitutes an important part of the phase noise. Therefore, it will affect the phase coherence between the channels, and is important to consider. In multicore fiber, the different spatial channels will experience completely uncorrelated phase noise since the surrounding WDM channels carry independent data in the different cores. In [Paper G] we investigated this effect and found that it causes penalties for joint-core carrier recovery.

For spectral superchannels, the situation is different. In fact, nonlinear phase noise is correlated over frequency [32], and it has been suggested that these correlations can be used to perform joint mitigation of XPM over low-baudrate subchannels

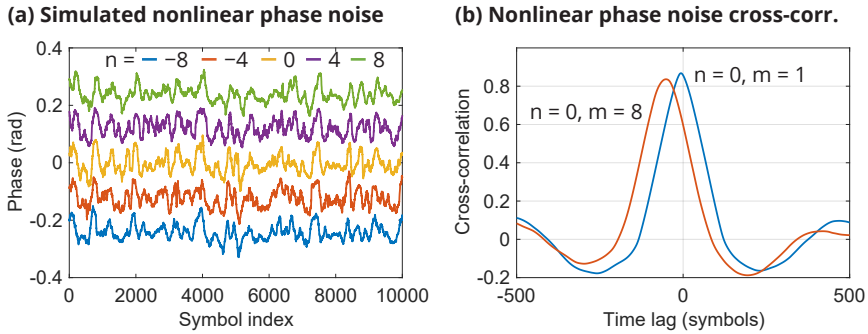

Figure 5.5: Split-step simulation of nonlinear phase noise in spectral superchannels. (a) Phase extracted from the phase tracking for different channel positions in the superchannel. $n = 0$ denotes the center channel (b) Cross-correlation of the phase noise from the center channel with its neighbor and the furthest channel. The simulated systems was a 17×20 GBd 64QAM superchannel transmitted over two 80 km spans. No laser phase noise was added, so the nonlinear phase noise is the only contribution. Launch power was 1 dBm per channel.

[94, 161]. In [Paper F] we demonstrated that the nonlinear phase noise contributions do not give significant penalties to master-slave carrier recovery schemes, and that joint phase estimation can increase the tolerance to nonlinearities. However, the correlations have not been studied over larger frequency separations.

The correlations of the nonlinear phase noise can be studied through split-step simulations. In Figure 5.5 the phase traces recovered from a 17×20 GBd superchannel are plotted and compared. In the simulation, no laser phase noise was considered, so the phase variations are only caused by nonlinear effects. The phase traces are visually similar but do have some differences. The cross-correlation shows that the highest correlation occurs for a time-shift between the phases corresponding roughly to the dispersive delay between the channels. This can be understood by the fact that the nonlinear effects occur mostly in the beginning of the span, when the signal power is high. This is consistent with the observations in [162], where the authors show that the low-frequency part of the transfer function for XPM [163, 164] varies only little with the spectral distance to the interfering channel. Low frequency in this context refers to approximately below 500 MHz, which matches the tracking capabilities of standard phase trackers. Indeed, in [162] joint electro-optical compensation of nonlinear phase noise was performed for 5 WDM channels.

5.4 Discussion

In this chapter we have discussed spectral and spatial superchannels, focusing on their phase-coherent properties, which follows from using a shared carrier for the subchannels. For spectral superchannels this means that an optical frequency comb supplies the carriers. The importance of the phase-coherence is that carrier recovery can be performed jointly over several channels. Joint methods for carrier recovery are discussed in Chapter 6.

Chapter 6

Joint carrier recovery

Transmitting and receiving several channels together opens the possibility to process them together. The situations where this can be beneficial can be divided into two categories. The first is when the channels suffer from the same impairments, caused either by non-ideal components shared between the channels, or by correlated transmission impairments. The second is when the channels couple into each other through linear or nonlinear processes, causing crosstalk. In this chapter we focus on joint carrier recovery, which belongs to the first category and relies on correlated phase noise. We will discuss methods both in the digital and analog domain.

6.1 Joint digital carrier recovery

If several channels share similar phase noise, this shared information can be utilized to make the phase-tracking more efficient. This is possible already in polarization-multiplexed systems [165] as long as the polarizations share the same transmitter and local-oscillator (LO) laser, which is typically the case. Spatial-division multiplexing (SDM) and frequency-comb based superchannels enables this concept to be extended to a much larger number of channels and have the potential to give large performance gains and complexity savings. In this section several different methods for joint carrier recovery are described, together with some practical considerations for managing limited phase coherence between the channels.

The term *joint carrier recovery* is often used loosely to describe all carrier recovery schemes that process several channels together, but includes two main categories that have quite different principles and benefits. These schemes are illustrated in Figure 6.1 and compared to standard, independent carrier recovery. The first scheme

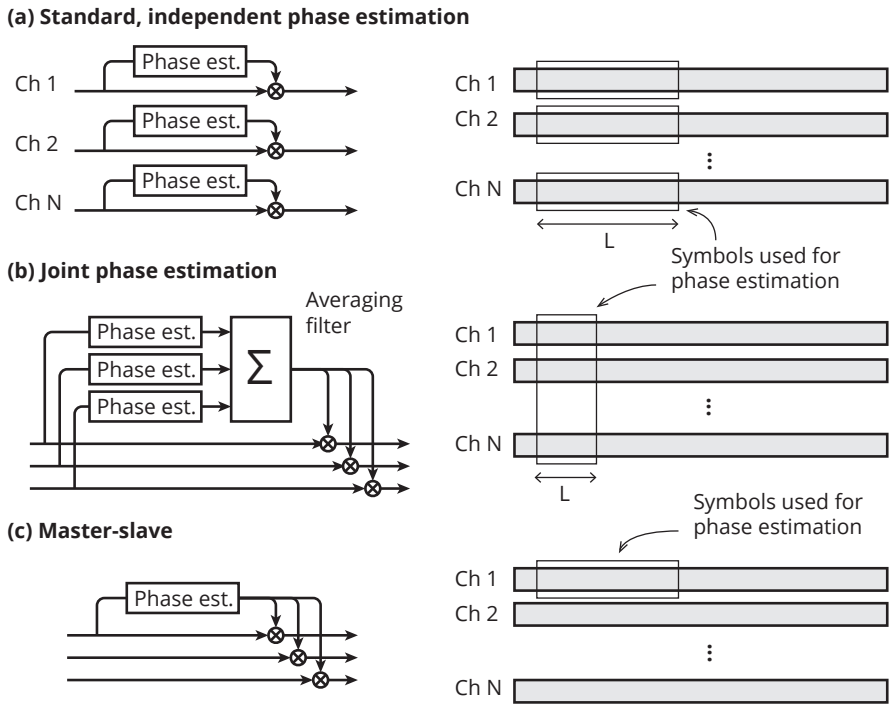

Figure 6.1: Comparison of (a) Standard, independent carrier recovery, where the phase noise is estimated from each channels separately. (b) Joint phase estimation, where the phase noise is estimated from all channels jointly. (c) Master-slave phase recovery, where the phase noise is estimated from one channel and reused for the other channels.

is joint phase *estimation*, where the phase information from all channels is used to estimate their common phase noise. In contrast with joint estimation is what is best described as *master-slave* schemes, where the phase noise is estimated from one channel—the master channel—and then used to compensate the phase noise of all the other channels. This scheme was proposed in [99] and used in [159], [Paper F] and [Paper G]. In joint-estimation schemes the shared information is utilized to provide a better phase estimate, for example by replacing time-averaging with averaging over channels, which improves the tracking speed. In contrast, master-slave schemes do not strive to improve the performance but instead to reduce the overall hardware effort. A third alternative that falls into neither of the above categories is to utilize the phase coherence to mitigate cycle slips by comparing the independently recov-

ered phase traces and detecting jumps above a certain threshold [166].

6.1.1 Joint estimation

The blind phase estimation schemes presented in Chapter 4 can relatively easily be extended to several channels by including single-symbol estimates from several channels in the time-averaging filters, as illustrated in Figure 6.1. This is described for the Viterbi-Viterbi algorithm in [167–169], and for BPS in [72] and [Paper C], and for a decision-directed feedback method in [143]. The inclusion of additional symbols in the averaging increases the signal-to-noise ratio (SNR) of the phase estimate, and the the filter length L can be reduced while still maintaining the same tolerance to Gaussian noise. In this way the tracking speed can be increased. The filtering may use different weights for the phase contributions from different channels if they have different amounts of additive noise [167, 168]. Depending on the type of algorithm used, the averaging might be performed on some intermediate stage, before the final phase is estimated.

It should be noted that a performance increase can only be expected if the system otherwise is limited by phase noise. While a performance increase was demonstrated with a high-linewidth laser in [143], modern coherent systems are not limited by laser phase noise, which explains the moderate performance gains from joint phase-estimation we observed in [Paper C]. Nonlinear phase noise however varies rapidly and may be more efficiently tracked using joint methods. This was first demonstrated for joint-polarization methods [167], but we found that it is also possible to do in spectral superchannels [Paper F].

Also pilot-symbol-based phase estimation can be extended to several channels, described for joint-polarization processing in [170] and joint-core processing in [171–173]. In pilot-based phase estimation there is a trade-off between performance and pilot-symbol rate, where a larger fraction of pilot-symbols leads to a higher tolerance to phase noise at the cost of spectral efficiency. When many channels are jointly processed, the fraction of pilots can be reduced while maintaining the same phase noise tolerance.

6.1.2 Master-slave carrier recovery

The principle for master-slave carrier recovery is straightforward. Frequency offset and phase estimation is performed as in the single-channel case on the master channel, and the resulting phase information is applied to slave channels through complex multiplication. As long as any inter-channel phase differences are compensated or negligible, performance will be the same as for independent carrier recovery.

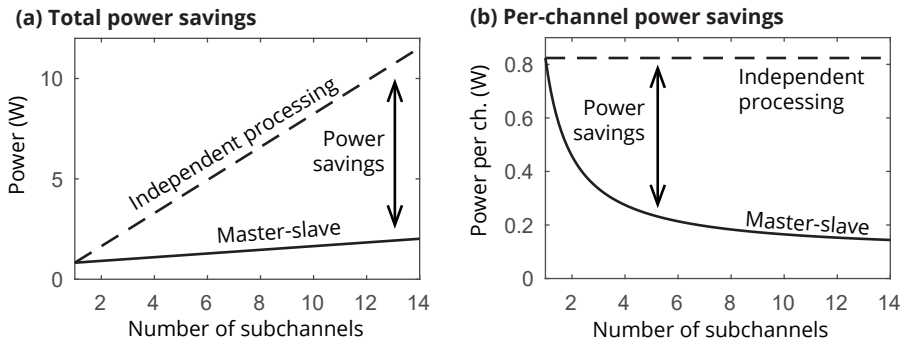

Figure 6.2: Two ways of quantifying power consumption saving through master slave carrier recovery. (a) shows the *total* power consumption (b) shows the *per-channel* power consumption. Numbers from [Paper E] for 40 GBd 64QAM.

How much reduction of computational complexity is possible to achieve will depend on the algorithm used and more specifically the relation between the complexity of the estimation and the compensation parts. In [Paper E], we evaluated the possible power consumption savings through an application-specific integrated circuit (ASIC) implementation of a blind phase-search (BPS) algorithm. This showed that quite significant power consumption reductions are indeed possible, but also that the remaining processing needed on the slave channels (essentially multiplying each symbol with the estimated phase from the master) had a not insignificant power consumption. This can be analyzed as follows: Assume that the power consumption of a phase recovery block can be divided into (a) the estimation power consumption P_{est}, which is the power consumption needed to estimate the phase noise from the signal, and (b) a compensation part P_{comp}, which is the power consumption of applying the estimated phase to the signal. Then, the power consumption of a conventional, independent phase recovery is simply

$$P_{\text{ind}} = N_{\text{ch}}(P_{\text{est}} + P_{\text{comp}}), \tag{6.1}$$

where N_{ch} is the number of channels. The power consumption of a master-slave phase recovery is instead

$$P_{\text{MS}} = P_{\text{est}} + N_{\text{ch}} P_{\text{comp}}. \tag{6.2}$$

Using the numbers we found in [Paper E] for 40 GBd 64QAM, the total power consumption savings can be estimated (plotted in Figure 6.2(a)). For example, in a system with 10 subchannels, several watts can be saved, which may be significant if

compared to the allowable power consumption of 18 W for a 100Gbit/s CFP2 module [12]. However, a 10×40 GBd PM-64QAM superchannel can carry more than 4 Tbit/s, so the comparison is not completely fair. Instead, it is interesting to normalize the power consumption and study the per-channel power consumption channel (which is proportional to e.g. the energy per bit). For independent processing, the power-per-channel is constant, and for master-slave processing it decreases as $1/N$ asymptotically towards P_{comp}. For the case with many jointly processed channels, the power savings per channel approaches 0.7 W in the example (plotted in Figure 6.2(b)).

Both perspectives can be relevant. The total power consumption is important from the perspective of transceiver integration, since the allowable total power consumption and heat generation is often limited for a given module form factor [12]. The normalized power consumption, maybe most useful in the form J/bit or W/100G, is on the other hand useful to compare power consumption for systems with different data throughput.

When discussing power consumption savings, it is important to consider the limitations of the power consumption estimates. The power consumption values used in the above discussion (from [Paper E]) are estimated from a circuit implementation of a BPS algorithm. While this kind of estimate is typically very accurate, they are also limited to one specific implementation of one algorithm. For example, a recent comparison of BPS and a pilot-aided method showed that BPS consumes around 10 time the power of the pilot-aided method [174]. Furthermore, the simple model for the power consumption of master-slave carrier recovery introduced above does not include any power consumption associated with distributing the phase information physically across the DSP circuit, which would affect the results.

6.1.3 Inter-channel phase differences

Joint carrier recovery methods are affected by phase differences between channels. Depending on the type of method, the effect of phase differences can be more or less critical. The sophisticated pilot-symbol-based method described in [173] is designed to take phase differences into account, and can make use of also relatively low correlation between the phase noise of the different channels. However, for blind joint phase estimation methods the phase differences should ideally be compensated before the main joint estimation stage so that the differences do not impact the joint estimation. However, the phase differences cannot be easily estimated before the common phase noise has been compensated. For this situation, decision-directed feedback methods are useful, as we used in [Paper C] and [Paper F]. In this method, the phase error of the channels is estimated individually after the joint phase estimation and compensation and used to find a correction phase applied individually

before the joint phase estimation.

For master-slave carrier recovery difference compensation is less critical, but as any phase differences will remain on the slave channels and cause a penalty it is desirable to compensate them. Since the motivation for using master-slave carrier recovery generally is complexity reduction, the critical issue is instead the complexity of how the phase difference are estimated and compensated. Any additional processing needed on the slave channels will reduce the possible complexity savings, so the phase difference compensation needs be kept at a minimum. The most attractive solution for this is to integrate the carrier recovery with the main adaptive equalizer that perform polarization demultiplexing and compensation of polarization mode dispersion (PMD). If a decision-directed algorithm is used, the equalizer will be able to track slow phase variations remaining on the slave channel, if the master phase is applied inside of the equalizer loop. We used this method in [Paper F] and [Paper G].

6.1.4 Effects of an optical delay between channels

Different optical delay of the jointly processed channels is a limiting factor for joint phase-compensation. This is not easily mitigated electronically since the phase noise on the detected signal is a sum of the phase noise from both the transmitter and LO lasers. Since only the phase noise of the transmitter laser will be delayed, the phase noise of the detected signals will not just be delayed versions of one another. This situation is illustrated in Figure 6.3. Sources of delay can be path length differences in optical components, but also chromatic dispersion in comb-based systems, inter-core skew in multicore systems and differential group delay in multimode systems. This will effectively limit the transmission distance for which joint processing is reasonable.

To further understand the effect of optical delays, consider a master-slave system with perfectly correlated carrier and LOs, except for an optical time delay of the slave channel. The master channel phase noise can then be written as a sum of the phase noise of the carrier and LO lines

$$\theta_M(t) = \theta_{\mathrm{C}}(t) + \theta_{\mathrm{LO}}(t). \tag{6.3}$$

which can be modeled as Wiener processes with variance parameters σ_C^2 and σ_{LO}^2 respectively. The slave is delayed with a time T before detection, so its phase noise can be written

$$\theta_S(t) = \theta_{\mathrm{C}}(t-T) + \theta_{\mathrm{LO}}(t). \tag{6.4}$$

Now, assuming that the phase estimate $\hat{\theta}_M(t)$ for the master channel is a perfect estimate of the actual phase $\hat{\theta}_M(t) = \theta_{\mathrm{C}}(t) + \theta_{\mathrm{LO}}(t)$, the remaining phase on the slave

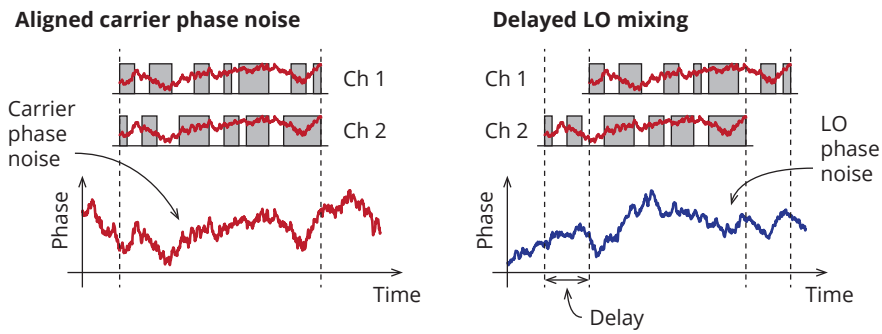

Figure 6.3: Illustration of the effect of optical delay on phase noise correlations. To the right, before delay, the carrier phase noise is aligned in the two channels. To the left, the channels have been skewed in time. This means that the addition of the LO phase noise will be delayed for one of the channels, causing phase noise differences that cannot be undone with electronics delays.

channel is

$$\theta'_S(t) = \theta_S(t) - \hat{\theta}_M(t) = \theta_C(t-T) - \theta_C(t). \tag{6.5}$$

In general, if $\theta(t)$ is a Wiener process with variance parameter σ^2, $\theta(t) - \theta(t-T)$ is a random Gaussian variable with zero mean and variance $\sigma^2|T|$ [72, 175]. Thus, the remaining phase noise in Eq. (6.5) is a random Gaussian variable with zero mean and variance

$$\mathrm{var}(\theta'_S(t)) = |T|\sigma_C^2. \tag{6.6}$$

Therefore, the variance of the remaining phase noise on the slave channel is proportional to both the variance parameter of the carrier laser and the time delay between the slave channel and the master channel. If instead the master phase was delayed electronically with T, the remaining phase would be

$$\theta'_S(t) = \theta_S(t) - \hat{\theta}_M(t-T_n) = \theta_{\mathrm{LO}}(t) - \theta_{\mathrm{LO}}(t-T), \tag{6.7}$$

which if the carrier and LO lasers have the same phase noise properties ($\sigma_C^2 = \sigma_{\mathrm{LO}}^2$) would give the same penalty on the slave channel. Similar considerations appear in phase tracking algorithms where the estimated phase for some reason needs to be delayed before being applied to the signal, e.g., in feedback phase estimation methods limited by parallelization [72]. It also needs to be considered in self-homodyne systems [175, 176] and when regenerating frequency combs from two lines [146].

6.2 Pilot tone-based carrier recovery

Digital carrier recovery can be significantly simplified or completely removed if one or several pilot tones are multiplexed with the data-carrying signals. In the first demonstrations of this method, the signal was polarization multiplexed with an unmodulated carrier [177–179]. At the receiver, the polarization is aligned and the pilot tone is used as the LO. This is known as *self-homodyne* detection. Alternatively, the signal and pilot tone can be detected with a Stokes polarimeter [180, 181] which enables digital polarization tracking. Such pilot-tone-based schemes can tolerate very high laser linewidths and also cancel nonlinear phase distortions [182]. In addition, digital carrier recovery can be omitted. However, since the pilot tone is transmitted on one of the polarizations, the spectral efficiency is reduced by a factor of two. In addition, ASE noise is added to the pilot tone during transmission, which leads to an OSNR penalty [183]. This effect can be partly reduced by filtering of the pilot tone [182].

The drawback of pilot tone-based carrier recovery is that the spectral efficiency is decreased to the overhead associated with the pilot tone. This is particularly severe in the case with a polarization multiplexed pilot tone, since the possible data throughput is reduced by a factor of two. Using multicore fiber (MCF), the overhead can be reduced by transmitting the pilot tone on a separate fiber core [158]. Since the pilot tone can be shared between all the cores, the reduction in spectral efficiency is not as prominent as when the pilot tone is polarization multiplexed with the signal.

The pilot tone can also be transmitted on a different frequency from the signal, either inserted electronically before modulation [184, 185] or in frequency-comb-based systems by leaving one or several comb lines unmodulated [138, 146–149]. In the latter systems, the LO frequency comb is phase locked to the transmitter comb, enabling self-homodyne detection. Since the full phase and frequency properties of the transmitter comb can be extracted from only two comb lines, the pilot-tone overhead can be kept low.

The pilot tone can also be detected using a coherent receiver [184] and the self-homodyne mixing performed digitally, which is known as *digital self-homodyne* detection [186] or *shared carrier reception* [176, 187]. The advantages of detecting the pilot tone digitally is that polarization tracking and pilot-tone filtering can be performed digitally. In [Paper B] digital self-homodyne detection was used.

Chapter 7

Future outlook

In this chapter, some interesting topics for further research related to this thesis are discussed.

Joint signal processing for nonlinearity mitigation

In thesis, it was demonstrated that joint phase estimation can be used to compensate the phase noise part of inter-channel nonlinear interference. Potentially, higher orders of nonlinear interference could also benefit from joint treatment. However, this depends on the correlation properties, which have not been studied in detail. Furthermore, new algorithms would need to be developed.

Optical frequency comb based systems

There are many interesting questions remaining relating to the use of optical frequency combs in multi-wavelength transceivers.

- One the assumptions behind the potential application of joint carrier-recovery methods is that the receivers for the involved channels should be co-integrated. For this purpose, an integrated, or at least compact, comb source is highly desirable. However, so far, joint carrier-recovery has not been demonstrated with other than bench-top electro-optical frequency combs. Therefore, it would be highly interesting to investigate joint carrier recovery using compact comb sources such as microresonator combs or semiconductor mode-locked lasers. A further possibility is to use integrated electro-optical frequency combs.

- The joint carrier-recovery methods demonstrated in this thesis essentially assumed that all comb lines had the same phase noise, which is not the full picture since frequency combs also have a line dependent phase noise term. However, as described in Eq. 5.7, ideally only two comb-lines are needed to estimate the full frequency and phase-noise properties of the comb. Joint carrier recovery using these relations have not been demonstrated. Apart from the theoretical beauty of such a scheme, this could potentially enable the use of comb sources with a high line-dependent phase noise for joint carrier recovery.
- A full-system approach needs to be taken to determine how the use of optical frequency combs will affect the overall power consumption. Even if the DSP power consumption can be decreased, the comb generation process is associated with some power consumption which needs to be accounted for. Optical frequency combs can also lead to power savings since they take the place of individual transmitter and LO lasers. This would also require some power consumption models for different comb sources to be developed.

Power consumption of broadband Raman amplification

In [Paper A] we investigated the trade-offs related to the power consumption when Raman amplification is used to increase the OSNR of the signal. However, Raman amplification can also be used to enable amplification over a wider bandwidth than in EDFA-based systems. This can be used to increase to capacity of a single fiber, which could be more energy efficient than adding an extra fiber.

DSP power consumption modelling

There are many interesting research questions involving power consumption trade-offs between DSP and other parts of the system. The work on these issues are currently limited by the lack of accurate DSP power consumption models that do not involve designing a full ASIC. Developing such models would enable more accurate predictions of the overall power consumption.

Chapter 8

Summary of papers

Paper A

Power Consumption Analysis of Hybrid EDFA/Raman Amplifiers in Long-Haul Transmission Systems,

Lars Lundberg, Peter A. Andrekson and Magnus Karlsson

Journal of Lightwave Technology, vol. 35, no. 11, pp. 2132–2142, 2017.

Here we analyze the power consumption of optical amplifiers and trade-offs between this and signal quality in terms of OSNR. We study both EDFAs and backwards pumped Raman amplification, and include also the power consumption of monitoring and management electronics. We find that the value of power consumption of the monitoring and management electronics significantly affects which system configuration gives the lowest power consumption.

We also study the impact modulation format and choice of FEC scheme has on the energy consumption per bit. We find that 16QAM is more energy efficient than QPSK, and that there are cases when it might be more energy efficient to increase the signal quality by shortening the spans instead of using a powerful FEC scheme.

My contribution: I performed theoretical and numerical modelling and wrote the paper.

Paper B

Power Consumption of a Minimal-DSP Coherent Link with a Polarization Multiplexed Pilot-Tone,

Lars Lundberg, Peter A. Andrekson and Magnus Karlsson

European Conference on Optical Communication (ECOC), Düsseldorf, Germany, paper Th.2.P2.SC5.58, 2016.

As the demand for bandwidth increase also for short systems, coherent technologies become more attractive also for this kind of links. Then, as length-dependent impairments no longer need to be compensated for in DSP, the power consumption trade-offs become different. In this paper, we study the power consumption of a link with minimal DSP aided by a polarization-multiplexed pilot-tone. The DSP power consumption is estimated by scaling values from a similar structure ASIC implementation. We find that the system power consumption is dominated by the optical components.

My contribution: I came up with the idea together with CF and performed the experiments. I analyzed the power consumption numbers produced by CF and put them into a system context. I wrote the paper together with CF and presented it at ECOC.

Paper C

Frequency Comb-Based WDM Transmission Systems Enabling Joint Signal Processing,

Lars Lundberg, Magnus Karlsson, Abel Lorences-Riesgo, Mikael Mazur, Victor Torres-Company, Jochen Schröder and Peter A. Andrekson

Applied Sciences, vol. 8, no. 5, p. 718, 2018.

This paper is an invited review of frequency comb-based transmission systems, focusing on how comb properties such as stable line spacing and phase coherence can be exploited in coherent optical communication systems.

My contribution: I wrote the section on joint DSP and planned and performed the experiments reported there with support from MM and ALR. I took the overall responsibility in managing the manuscript and wrote the conclusions.

Paper D

Phase Correlation Between Lines of Electro-Optical Frequency Combs

Lars Lundberg, Mikael Mazur, Attila Fülöp, Victor Torres-Company, Magnus Karlsson, and Peter A. Andrekson

Conference on Lasers and Electro-Optics (CLEO), San José, California, USA, 2018.

In this paper we measure the phase variations of the lines of electro-optical frequency combs using the multiheterodyne technique. This way we can simultaneously measure 49 comb lines and study the coherence properties. We find that the phase-noise has a correlation of over 99.99%. In addition, also the phase difference between the lines is correlated.

My contribution: I planned and performed the experiment with support from MM. I processed and analyzed the measurements. I wrote the paper and presented it at CLEO.

Paper E

Power Consumption Savings Through Joint Carrier Recovery for Spectral and Spatial Superchannels,

Lars Lundberg, Erik Börjeson, Christoffer Fougstedt, Mikael Mazur, Magnus Karlsson, Peter A. Andrekson and Per Larsson-Edefors

European Conference on Optical Communication (ECOC), Rome, Italy, 2018.

This paper is based on analyzing the power consumption number from an ASIC implementation of a blind phase search algorithm for carrier recovery. Using these numbers, we estimate the possible power consumption savings associated with master-slave carrier recovery. We find that the slave power consumption is 27% of master power for 16QAM and 13% for 64QAM, which enables power savings of up to 0.7 W per channel for 40 GBd PM-64QAM.

My contribution: The ASIC implementation was made by EB as his master thesis project. I supervised EB together with CF and PLE, chose the test cases in the paper, and analyzed the ASIC power consumption numbers in a system context. I performed the experiments with support from MM. I wrote the paper and presented it at ECOC.

Paper F

Phase-coherent lightwave communications with frequency combs

Lars Lundberg, Mikael Mazur, Ali Mirani, Benjamin Foo, Jochen Schröder, Victor Torres-Company, Magnus Karlsson and Peter A. Andrekson

Submitted to *Science*, 2019.

In this paper we experimentally demonstrate joint carrier recovery for optical frequency comb-based transmission. We show that master-slave carrier recovery is possible for a 23×20 GBd PM-64QAM superchannel transmitted up to 160 km. We also show that joint-phase estimation can increase the tolerance to inter-channel nonlinear interference.

My contribution: I and MM jointly designed the experimental setup and built it with assistance from AM. I designed the joint digital processing methods and analyzed the data. I wrote the paper together with VTC, JS and MK.

Paper G

Master-slave carrier recovery for M-QAM multicore fiber transmission

Lars Lundberg, Benjamin J. Puttnam, Rubin S. Luís, Georg Rademacher, Magnus Karlsson, Peter A. Andrekson, Yoshinari Awaji, and Naoya Wada

Submitted to *Optics Express*, 2019.

In this paper we experimentally and numerically investigate master-slave carrier recovery for WDM multicore transmission in the presence of nonlinear interference and inter-core skew. We find that inter-channel nonlinear interference causes a moderate penalty on the slave channels. Furthermore, we find that inter-core skew occurring naturally in multicore fiber causes penalties if left uncompensated.

My contribution: The experimental part of this paper was carried out during my visit to the National Institute of Information and Communications Technology (NICT) in Tokyo, Japan. I planned the experiment and performed the measurements together with BJP, RSL and GR. I designed the joint digital processing methods and analyzed the data. I performed the simulations and wrote the paper.

Bibliography

[1] "World internet users statistics," https://www.internetworldstats.com/stats.htm, accessed 2019-03-03.

[2] K. Kao and G. Hockham, "Dielectric-fibre surface waveguides for optical frequencies," *Proceedings of the Institution of Electrical Engineers*, vol. 113, no. 7, pp. 1151–1158, 1966.

[3] T. H. Maiman, "Stimulated Optical Radiation in Ruby," *Nature*, vol. 187, no. 4736, pp. 493–494, 1960.

[4] R. Mears, L. Reekie, I. Jauncey, and D. Payne, "Low-noise erbium-doped fibre amplifier operating at 1.54μm," *Electronics Letters*, vol. 23, no. 19, pp. 1026–1028, 1987.

[5] H. Sun, K.-T. Wu, and K. Roberts, "Real-time measurements of a 40 Gb/s coherent system," *Optics Express*, vol. 16, no. 2, pp. 873–879, 2008.

[6] C. E. Shannon, "A Mathematical Theory of Communication," *Bell System Technical Journal*, vol. 27, no. 3, pp. 379–423, 1948.

[7] M. J. Golay, "Notes on digital coding," *Proceedings of the Institute of Radio Engineers*, vol. 37, no. 6, pp. 657–657, 1949.

[8] R. W. Hamming, "Error Detecting and Error Correcting Codes," *Bell System Technical Journal*, vol. 29, no. 2, pp. 147–160, 1950.

[9] R. S. Tucker, "Green optical communications–Part I: Energy limitations in transport," *IEEE Journal of Selected Topics in Quantum Electronics*, vol. 17, no. 2, pp. 245–260, 2011.

[10] D. C. Kilper, G. Atkinson, S. K. Korotky, S. Goyal, P. Vetter, D. Suvakovic, and O. Blume, "Power Trends in Communication Networks," *IEEE Journal of Selected Topics in Quantum Electronics*, vol. 17, no. 2, pp. 275–284, 2011.

[11] "Climate Change 2013: The Physical Science Basis," Intergovernmental Panel on Climate Change (IPCC), 2013.

[12] J. C. Geyer, C. Rasmussen, B. Shah, T. Nielsen, and M. Givehchi, "Power efficient coherent transceivers," in *European Conference on Optical Communication (ECOC)*, 2016.

[13] "HIS Infonetics 100G+ Coherent Optical Equipment Ports Mannual Market Share Size and Forecasts," 2015. [Online]. Available: http://news.ihsmarkit.com/press-release/technology/ihs-forecasts-huge-growth-100-gigabit-optical-ports-operators-increase-netw

[14] X. Zhou and H. Liu, "Pluggable DWDM: Considerations For Campus and Metro DCI Applications," in *European Conference on Optical Communication (ECOC)*, 2016, presented at WS 3: Short range optical transmission for emrging 5G fronthaul, DCI and Metro networks. [Online]. Available: https://static.googleusercontent.com/media/research.google.com/en//pubs/archive/45713.pdf

[15] X. Liu, S. Chandrasekhar, and P. J. Winzer, "Digital Signal Processing Techniques Enabling Multi-Tb/s Superchannel Transmission: An overview of recent advances in DSP-enabled superchannels," *IEEE Signal Processing Magazine*, vol. 31, no. 2, pp. 16–24, 2014.

[16] P. J. Winzer and D. T. Neilson, "From Scaling Disparities to Integrated Parallelism: A Decathlon for a Decade," *Journal of Lightwave Technology*, vol. 35, no. 5, pp. 1099–1115, 2017.

[17] S. Chandrasekhar, X. L. X. Liu, B. Zhu, and D. W. Peckham, "Transmission of a 1.2-Tb/s 24-carrier no-guard-interval coherent OFDM superchannel over 7200-km of ultra-large-area fiber," *European Conference on Optical Communication (ECOC)*, 2009.

[18] D. J. Richardson, J. M. Fini, and L. E. Nelson, "Space-division multiplexing in optical fibres," *Nature Photonics*, vol. 7, no. 5, pp. 354–362, 2013.

[19] "Neophotonics ITLA," https://www.neophotonics.com/product/itla/, accessed: 2017-07-29.

[20] B. S. G. Pillai, B. Sedighi, K. Guan, N. P. Anthapadmanabhan, W. Shieh, K. J. Hinton, and R. S. Tucker, "End-to-end energy modeling and analysis of long-haul coherent transmission systems," *Journal of Lightwave Technology*, vol. 32, no. 18, pp. 3093–3111, 2014.

[21] K.-P. Ho and H.-W. Cuei, "Generation of arbitrary quadrature signals using one dual-drive Modulator," *Journal of Lightwave Technology*, vol. 23, no. 2, pp. 764–770, 2005.

[22] K.-P. Ho, *Phase-modulated optical communication systems*. Springer Science & Business Media, 2005.

[23] S. S. Azadeh, F. Merget, S. Romero-García, A. Moscoso-Mártir, N. von den Driesch, J. Müller, S. Mantl, D. Buca, and J. Witzens, "Low Vπ Silicon photonics modulators with highly linear epitaxially grown phase shifters," *Optics Express*, vol. 23, no. 18, pp. 23 526–23 550, 2015.

[24] R. Nagarajan, M. Kato, J. Pleumeekers, P. Evans, S. Corzine, S. Hurtt, A. Dentai, S. Murthy, M. Missey, R. Muthiah, R. A. Salvatore, C. Joyner, R. Schneider, M. Ziari, F. Kish, and D. Welch, "InP Photonic Integrated Circuits," *IEEE Journal of Selected Topics in Quantum Electronics*, vol. 16, no. 5, pp. 1113–1125, 2010.

[25] S. J. Savory, "Digital Coherent Optical Receivers: Algorithms and Subsystems," *IEEE Journal of Selected Topics in Quantum Electronics*, vol. 16, no. 5, pp. 1164–1179, 2010.

[26] B. P. Ginsburg and A. P. Chandrakasan, "Dual Time-Interleaved Successive Approximation Register ADCs for an Ultra-Wideband Receiver," *IEEE Journal of Solid-State Circuits*, vol. 42, no. 2, pp. 247–257, 2007.

[27] D. A. Morero, M. A. Castrillon, A. Aguirre, M. R. Hueda, and O. E. Agazzi, "Design Tradeoffs and Challenges in Practical Coherent Optical Transceiver Implementations," *Journal of Lightwave Technology*, vol. 34, no. 1, pp. 121–136, 2016.

[28] B. S. G. Pillai, B. Sedighi, W. Shieh, and R. S. Tucker, "Chromatic Dispersion Compensation – An Energy Consumption Perspective," in *Optical Fiber Communication Conference (OFC)*, 2012, p. OM3A.8.

[29] E. Tipsuwannakul, J. Li, T. A. Eriksson, L. Egnell, F. Sjöström, J. Pejnefors, P. A. Andrekson, and M. Karlsson, "Influence of Fiber-Bragg Grating-Induced Group-Delay Ripple in High-Speed Transmission Systems," *Journal of Optical Communications and Networking*, vol. 4, no. 6, pp. 514–521, 2012.

[30] R. Dar, M. Feder, A. Mecozzi, and M. Shtaif, "Properties of nonlinear noise in long, dispersion-uncompensated fiber links," *Optics Express*, vol. 21, no. 22, pp. 25 685–25 699, 2013.

[31] ——, "Inter-Channel Nonlinear Interference Noise in WDM Systems: Modeling and Mitigation," *Journal of Lightwave Technology*, vol. 33, no. 5, pp. 1044–1053, 2015.

[32] M. Secondini and E. Forestieri, "On XPM Mitigation in WDM Fiber-Optic Systems," *IEEE Photonics Technology Letters*, vol. 26, no. 22, pp. 2252–2255, 2014.

[33] T. Fehenberger, M. Mazur, T. A. Eriksson, M. Karlsson, and N. Hanik, "Experimental Analysis of Correlations in the Nonlinear Phase Noise in Optical Fiber Systems," in *European Conference on Optical Communication (ECOC)*, 2016.

[34] M. P. Yankov, T. Fehenberger, L. Barletta, and N. Hanik, "Low-Complexity Tracking of Laser and Nonlinear Phase Noise in WDM Optical Fiber Systems," *Journal of Lightwave Technology*, vol. 33, no. 23, pp. 4975–4984, 2015.

[35] M. P. Yankov, F. Da Ros, E. P. da Silva, T. Fehenberger, L. Barletta, D. Zibar, L. K. Oxenlowe, M. Galili, and S. Forchhammer, "Nonlinear Phase Noise Compensation in Experimental WDM Systems With 256QAM," *Journal of Lightwave Technology*, vol. 35, no. 8, pp. 1438–1443, 2017.

[36] P. Poggiolini, "The GN Model of Non-Linear Propagation in Uncompensated Coherent Optical Systems," *Journal of Lightwave Technology*, vol. 30, no. 24, pp. 3857–3879, 2012.

[37] P. Johannisson and M. Karlsson, "Perturbation Analysis of Nonlinear Propagation in a Strongly Dispersive Optical Communication System," *Journal of Lightwave Technology*, vol. 31, no. 8, pp. 1273–1282, 2013.

[38] E. Agrell, A. Alvarado, G. Durisi, and M. Karlsson, "Capacity of a nonlinear optical channel with finite memory," *Journal of Lightwave Technology*, vol. 32, no. 16, pp. 2862–2876, 2014.

[39] A. Alvarado, E. Agrell, D. Lavery, R. Maher, and P. Bayvel, "Replacing the Soft-Decision FEC Limit Paradigm in the Design of Optical Communication Systems," *Journal of Lightwave Technology*, vol. 34, no. 2, pp. 707–721, 2016.

[40] A. Alvarado, T. Fehenberger, B. Chen, and F. M. J. Willems, "Achievable Information Rates for Fiber Optics: Applications and Computations," *Journal of Lightwave Technology*, vol. 36, no. 2, pp. 424–439, 2018.

[41] A. A. M. Saleh, R. M. Jopson, J. D. Evankow, and J. Aspell, "Modeling of gain in erbium-doped fiber amplifiers," *IEEE Photonics Technology Letters*, vol. 2, no. 10, pp. 714–717, 1990.

[42] R. M. Jopson and A. A. Saleh, "Modeling of gain and noise in erbium-doped fiber amplifiers," in *Proceedings of the SPIE*, vol. 1581, no. 2, 1992, pp. 114–119.

[43] P. C. Becker, N. A. Olsson, and J. R. Simpson, *Erbium-doped fiber amplifiers: fundamentals and technology*. San Diego: Academic Press, 1999.

[44] H. Kogelnik and A. Yariv, "Considerations of Noise and Schemes for Its Reduction in Laser Amplifiers," *Procedings of the IEEE*, vol. 52, no. 2, pp. 165–172, 1964.

[45] R. H. Stolen, W. J. Tomlinson, H. A. Haus, and J. P. Gordon, "Raman response function of silica-core fibers," *Journal of the Optical Society of America B*, vol. 6, no. 6, pp. 1159–1166, 1989.

[46] V. Curri and A. Carena, "Merit of Raman pumping in uniform and uncompensated links Supporting NyWDM transmission," *Journal of Lightwave Technology*, vol. 34, no. 2, pp. 554–565, 2016.

[47] C. Headley and G. P. Agrawal, *Raman amplification in fiber optical communication systems*. Elsevier Academic Press, 2005.

[48] V. Curri, A. Carena, P. Poggiolini, G. Bosco, and F. Forghieri, "Extension and validation of the GN model for non-linear interference to uncompensated links using Raman amplification," *Optics Express*, vol. 21, no. 3, pp. 3308–3317, 2013.

[49] W. S. Pelouch, "Raman amplification: An enabling technology for long-haul coherent transmission systems," *Journal of Lightwave Technology*, vol. 34, no. 1, pp. 6–19, 2016.

[50] D. Enescu and E. O. Virjoghe, "A review on thermoelectric cooling parameters and performance," *Renewable and Sustainable Energy Reviews*, vol. 38, pp. 903–916, 2014.

[51] L. A. Johnson, *Application note: Controlling temperatures of diode lasers and detectors thermoelectrically*, Newport Corporation, Accessed: 2016-11-07. [Online]. Available: https://www.newport.com/medias/sys_

master/images/images/hcc/hc7/8797049389086/
AN01-Controlling-Temperatures-of-Laser-Diodes-Thermoelectrically.pdf

[52] J. Yoshida, C. F. Hayamizu, H. Itoh, M. Miura, T. Sawamura, S. Irino, T. Takeuchi, T. Kimura, and N. Tsukiji, "2.8 FITs of Field Reliability of 1480nm/14xx-nm Pump Lasers," in *Optical Fiber Communication Conference (OFC)*, 2015, p. W2A.2.

[53] "Finisar fixed gain EDFA," https://www.finisar.com/sites/default/files/downloads/finisar_amplifier_fixed_gain_edfa_product_brief.pdf, accessed: 2017-07-18.

[54] S. Desbruslais, "Maximizing the capacity of ultra-long haul submarine systems," in *European Conference on Networks and Optical Communications (NOC)*, 2015.

[55] W. Van Heddeghem, F. Idzikowski, W. Vereecken, D. Colle, M. Pickavet, and P. Demeester, "Power consumption modeling in optical multilayer networks," *Photonic Network Communications*, vol. 24, no. 2, pp. 86–102, 2012.

[56] W. Van Heddeghem and F. Idzikowski, "Equipment power consumption in optical multilayer networks – source data," Tech. Rep., 2012. [Online]. Available: http://powerlib.intec.ugent.be/

[57] N. J. Doran and A. D. Ellis, "Minimising total energy requirements in amplified links by optimising amplifier spacing," *Optics Express*, vol. 22, no. 16, pp. 19 810–19 817, 2014.

[58] I. Fatadin, S. J. Savory, and D. Ives, "Compensation of Quadrature Imbalance in an Optical QPSK Coherent Receiver," *IEEE Photonics Technology Letters*, vol. 20, no. 20, pp. 1733–1735, 2008.

[59] S. J. Savory, "Digital filters for coherent optical receivers," *Optics Express*, vol. 16, no. 2, pp. 804–817, 2008.

[60] A. Sheikh, C. Fougstedt, A. Graell i Amat, P. Johannisson, P. Larsson-Edefors, and M. Karlsson, "Dispersion Compensation FIR Filter With Improved Robustness to Coefficient Quantization Errors," *Journal of Lightwave Technology*, vol. 34, no. 22, pp. 5110–5117, 2016.

[61] C. Fougstedt, A. Sheikh, P. Johannisson, A. Graell i Amat, and P. Larsson-Edefors, "Power-Efficient Time-Domain Dispersion Compensation Using Optimized FIR Filter Implementation," in *Signal Processing in Photonic Communications (SPPCOM)*, 2015, p. SpT3D.3.

[62] K. Kikuchi, “Clock recovering characteristics of adaptive finite-impulse-response filters in digital coherent optical receivers,” *Optics Express*, vol. 19, no. 6, pp. 5611–5619, 2011.

[63] D. Godard, “Self-Recovering Equalization and Carrier Tracking in Two-Dimensional Data Communication Systems,” *IEEE Transactions on Communications*, vol. 28, no. 11, pp. 1867–1875, 1980.

[64] K. Kikuchi, “Polarization-demultiplexing algorithm in the digital coherent receiver,” in *Digest of the IEEE/LEOS Summer Topical Meetings*, no. 9, 2008, pp. 101–102.

[65] W. Sethares, G. Rey, and C. Johnson, “Approaches to blind equalization of signals with multiple modulus,” in *International Conference on Acoustics, Speech, and Signal Processing*, 1989, pp. 972–975.

[66] M. Ready and R. Gooch, “Blind equalization based on radius directed adaptation,” in *International Conference on Acoustics, Speech, and Signal Processing*, 1990, pp. 1699–1702.

[67] J. Treichler, M. Larimore, and J. Harp, “Practical blind demodulators for high-order QAM signals,” *Proceedings of the IEEE*, vol. 86, no. 10, pp. 1907–1926, 1998.

[68] I. Fatadin, D. Ives, and S. Savory, “Blind Equalization and Carrier Phase Recovery in a 16-QAM Optical Coherent System,” *Journal of Lightwave Technology*, vol. 27, no. 15, pp. 3042–3049, 2009.

[69] A. J. Viterbi and A. M. Viterbi, “Nonlinear estimation of PSK-modulated carrier phase with application to burst digital transmission,” *IEEE Transactions on Information Theory*, vol. 29, no. 4, pp. 543–551, 1983.

[70] J. Barry and J. Kahn, “Carrier synchronization for homodyne and heterodyne detection of optical quadriphase-shift keying,” *Journal of Lightwave Technology*, vol. 10, no. 12, pp. 1939–1951, 1992.

[71] E. Ip and J. M. Kahn, “Feedforward Carrier Recovery for Coherent Optical Communications,” *Journal of Lightwave Technology*, vol. 25, no. 9, pp. 2675–2692, 2007.

[72] T. Pfau, S. Hoffmann, and R. Noé, “Hardware-Efficient Coherent Digital Receiver Concept With Feedforward Carrier Recovery for M-QAM Constellations,” *Journal of Lightwave Technology*, vol. 27, no. 8, pp. 989–999, 2009.

[73] D. E. Crivelli, M. R. Hueda, H. S. Carrer, M. del Barco, R. R. Lopez, P. Gianni, J. Finochietto, N. Swenson, P. Voois, and O. E. Agazzi, "Architecture of a Single-Chip 50 Gb/s DP-QPSK/BPSK Transceiver With Electronic Dispersion Compensation for Coherent Optical Channels," *IEEE Transactions on Circuits and Systems I: Regular Papers*, vol. 61, no. 4, pp. 1012–1025, 2014.

[74] I. Fatadin, D. Ives, and S. J. Savory, "Laser Linewidth Tolerance for 16-QAM Coherent Optical Systems Using QPSK Partitioning," *IEEE Photonics Technology Letters*, vol. 22, no. 9, pp. 631–633, 2010.

[75] S. K. Oh and S. P. Stapleton, "Blind phase recovery using finite alphabet properties in digital communications," *Electronics Letters*, vol. 33, no. 3, pp. 175–176, 1997.

[76] T. Pfau and R. Noé, "Phase-Noise-Tolerant Two-Stage Carrier Recovery Concept for Higher Order QAM Formats," *IEEE Journal of Selected Topics in Quantum Electronics*, vol. 16, no. 5, pp. 1210–1216, 2010.

[77] X. Zhou, "An improved feed-forward carrier recovery algorithm for coherent receiver with M-QAM modulation format," *IEEE Photonics Technology Letters*, vol. 22, no. 14, pp. 1051–1053, 2010.

[78] J. Li, L. Li, Z. Tao, T. Hoshida, and J. C. Rasmussen, "Laser-Linewidth-Tolerant Feed-Forward Carrier Phase Estimator With Reduced Complexity for QAM," *Journal of Lightwave Technology*, vol. 29, no. 16, pp. 2358–2364, 2011.

[79] X. Li, Y. Cao, S. Yu, W. Gu, and Y. Ji, "A Simplified Feedforward Carrier Recovery Algorithm for Coherent Optical QAM System," *Journal of Lightwave Technology*, vol. 29, no. 5, pp. 801–807, 2011.

[80] H. Sun, K.-T. Wu, S. Thomson, and Y. Wu, "Novel 16QAM carrier recovery based on blind phase search," in *European Conference on Optical Communication (ECOC)*, 2014.

[81] M. Xiang, S. Fu, L. Deng, M. Tang, P. Shum, and D. Liu, "Low-complexity feed-forward carrier phase estimation for M-ary QAM based on phase search acceleration by quadratic approximation," *Optics Express*, vol. 23, no. 15, pp. 19 142–19 153, 2015.

[82] W. Weber, "Differential Encoding for Multiple Amplitude and Phase Shift Keying Systems," *IEEE Transactions on Information Theory*, vol. 26, no. 3, pp. 385–391, 1978.

[83] J. C. Cartledge, F. P. Guiomar, F. R. Kschischang, G. Liga, and M. P. Yankov, "Digital signal processing for fiber nonlinearities," *Optics Express*, vol. 25, no. 3, p. 1916, 2017.

[84] E. Ip and J. M. Kahn, "Compensation of Dispersion and Nonlinear Impairments Using Digital Backpropagation," *Journal of Lightwave Technology*, vol. 26, no. 20, pp. 3416–3425, 2008.

[85] V. Parahyba, J. Reis, S. Ranzini, E. Schneider, E. Rosa, F. Simões, J. Diniz, L. Carvalho, E. Filho, J. Oliveira, and J. Oliveira, "Performance against implementation of digital backpropagation for high-speed coherent optical systems," *Electronics Letters*, vol. 51, no. 14, pp. 1094–1096, 2015.

[86] G. Gao, X. Chen, and W. Shieh, "Influence of PMD on fiber nonlinearity compensation using digital back propagation," *Optics Express*, vol. 20, no. 13, pp. 14 406–14 418, 2012.

[87] D. Rafique and A. D. Ellis, "Impact of signal-ASE four-wave mixing on the effectiveness of digital back-propagation in 112 Gb/s PM-QPSK systems," *Optics Express*, vol. 19, no. 4, pp. 3449–3454, 2011.

[88] R. Dar and P. J. Winzer, "On the Limits of Digital Back-Propagation in Fully Loaded WDM Systems," *IEEE Photonics Technology Letters*, vol. 28, no. 11, pp. 1253–1256, 2016.

[89] N. Fontaine, "Spectrally-sliced Coherent Receivers for THz Bandwidth Optical Communications," in *European Conference and Exhibition on Optical Communication (ECOC)*, 2013, pp. 24–26.

[90] R. Maher, T. Xu, L. Galdino, M. Sato, A. Alvarado, K. Shi, S. J. Savory, B. C. Thomsen, R. I. Killey, and P. Bayvel, "Spectrally Shaped DP-16QAM Super-Channel Transmission with Multi-Channel Digital Back-Propagation," *Scientific Reports*, vol. 5, no. 1, p. 8214, 2015.

[91] E. Temprana, E. Myslivets, B. P.-P. Kuo, L. Liu, V. Ataie, N. Alic, and S. Radic, "Overcoming Kerr-induced capacity limit in optical fiber transmission," *Science*, vol. 348, no. 6242, pp. 1445–1448, 2015.

[92] C. Fougstedt, M. Mazur, L. Svensson, H. Eliasson, M. Karlsson, and P. Larsson-Edefors, "Time-Domain Digital Back Propagation: Algorithm and Finite-Precision Implementation Aspects," in *Optical Fiber Communication Conference (OFC)*, 2017, p. W1G.4.

[93] C. Fougstedt, L. Svensson, M. Mazur, M. Karlsson, and P. Larsson-Edefors, "ASIC Implementation of Time-Domain Digital Back Propagation for Coherent Receivers," *IEEE Photonics Technology Letters*, vol. 30, no. 13, pp. 1179–1182, 2018.

[94] O. Golani, M. Feder, and M. Shtaif, "Equalization Methods for Out-of-Band Nonlinearity Mitigation in Fiber-Optic Communications," *Applied Sciences*, vol. 9, no. 3, p. 511, 2019.

[95] J.-X. Cai, H. G. Batshon, M. V. Mazurczyk, O. V. Sinkin, D. Wang, M. Paskov, W. W. Patterson, C. R. Davidson, P. C. Corbett, G. M. Wolter, T. E. Hammon, M. A. Bolshtyansky, D. G. Foursa, and A. N. Pilipetskii, "70.46 Tb/s Over 7,600 km and 71.65 Tb/s Over 6,970 km Transmission in C+L Band Using Coded Modulation With Hybrid Constellation Shaping and Nonlinearity Compensation," *Journal of Lightwave Technology*, vol. 36, no. 1, pp. 114–121, 2018.

[96] J.-x. Cai, H. G. Batshon, M. V. Mazurczyk, O. V. Sinkin, D. Wang, M. Paskov, C. R. Davidson, W. W. Patterson, A. Turukhin, M. A. Bolshtyansky, and D. G. Foursa, "51.5 Tb/s Capacity over 17,107 km in C+L Bandwidth Using Single-Mode Fibers and Nonlinearity Compensation," *Journal of Lightwave Technology*, vol. 36, no. 11, pp. 2135–2141, 2018.

[97] N. H. E. Weste and D. M. Harris, *CMOS VLSI Design: A Circuits and Systems Perspective*. Addisson-Wesley, 2011.

[98] C. Fougstedt, P. Johannisson, L. Svensson, and P. Larsson-Edefors, "Dynamic Equalizer Power Dissipation Optimization," in *Optical Fiber Communication Conference (OFC)*, 2016, p. W4A.2.

[99] M. D. Feuer, L. E. Nelson, X. Zhou, S. L. Woodward, R. Isaac, Benyuan Zhu, T. F. Taunay, M. Fishteyn, J. M. Fini, and M. F. Yan, "Joint Digital Signal Processing Receivers for Spatial Superchannels," *IEEE Photonics Technology Letters*, vol. 24, no. 21, pp. 1957–1960, 2012.

[100] S. A. Diddams, "An Optical Clock Based on a Single Trapped 199Hg+ Ion," *Science*, vol. 293, no. 5531, pp. 825–828, 2001.

[101] I. Coddington, W. Swann, and N. Newbury, "Coherent Multiheterodyne Spectroscopy Using Stabilized Optical Frequency Combs," *Physical Review Letters*, vol. 100, no. 1, p. 013902, 2008.

[102] P. Trocha, M. Karpov, D. Ganin, M. H. P. Pfeiffer, A. Kordts, S. Wolf, J. Krockenberger, P. Marin-Palomo, C. Weimann, S. Randel, W. Freude, T. J. Kippenberg, and C. Koos, "Ultrafast optical ranging using microresonator soliton frequency combs," *Science*, vol. 359, no. 6378, pp. 887–891, 2018.

[103] M.-G. Suh and K. J. Vahala, "Soliton microcomb range measurement," *Science*, vol. 359, no. 6378, pp. 884–887, 2018.

[104] D. J. Jones, S. A. Diddams, J. K. Ranka, A. Stentz, R. S. Windeler, J. L. Hall, and S. T. Cundiff, "Carrier-Envelope Phase Control of Femtosecond Mode-Locked Lasers and Direct Optical Frequency Synthesis," *Science*, vol. 288, no. 5466, pp. 635–639, 2000.

[105] J. Li, X. Yi, H. Lee, S. A. Diddams, and K. J. Vahala, "Electro-optical frequency division and stable microwave synthesis," *Science*, vol. 345, no. 6194, pp. 309–313, 2014.

[106] T. Morioka, H. Takara, S. Kawanishi, O. Kamatani, K. Takiguchi, K. Uchiyama, M. Saruwatari, H. Takahashi, M. Yamada, T. Kanamori, and H. Ono, "1 Tbit/s (100 Gbit/s $\times$ 10 channel) OTDM/WDM transmission using a single supercontinuum WDM source," *Electronics Letters*, vol. 32, no. 10, pp. 906–907, 1996.

[107] J. Veselka and S. Korotky, "A multiwavelength source having precise channel spacing for WDM systems," *IEEE Photonics Technology Letters*, vol. 10, no. 7, pp. 958–960, 1998.

[108] H. Takara, T. Ohara, K. Mori, K.-I. Sato, E. Yamada, Y. Inoue, T. Shibata, M. Abe, T. Morioka, and K.-I. Sato, "More than 1000 channel optical frequency chain generation from single supercontinuum source with 12.5 GHz channel spacing," *Electronics Letters*, vol. 36, no. 25, pp. 2089–2090, 2000.

[109] H. Takara, T. Ohara, and K. Sato, "Over 1000 km DWDM transmission with supercontinuum multi-carrier source," *Electronics Letters*, vol. 39, no. 14, pp. 1078–1079, 2003.

[110] H. Takara, H. Masuda, K. Mori, K. Sato, Y. Inoue, T. Ohara, A. Mori, M. Kohtoku, Y. Miyamoto, T. Morioka, and S. Kawanishi, "124 nm seamless bandwidth, 313$\times$10 Gbit/s DWDM transmission," *Electronics Letters*, vol. 39, no. 4, pp. 382–383, 2003.

[111] T. Ohara, H. Takara, T. Yamamoto, H. Masuda, T. Morioka, M. Abe, and H. Takahashi, "Over-1000-channel ultradense WDM transmission with supercontinuum multicarrier source," *Journal of Lightwave Technology*, vol. 24, no. 6, pp. 2311–2317, 2006.

[112] D. Hillerkuss, R. Schmogrow, T. Schellinger, M. Jordan, M. Winter, G. Huber, T. Vallaitis, R. Bonk, P. Kleinow, F. Frey, M. Roeger, S. Koenig, A. Ludwig, A. Marculescu, J. Li, M. Hoh, M. Dreschmann, J. Meyer, S. Ben Ezra, N. Narkiss, B. Nebendahl, F. Parmigiani, P. Petropoulos, B. Resan, A. Oehler, K. Weingarten, T. Ellermeyer, J. Lutz, M. Moeller, M. Huebner, J. Becker, C. Koos, W. Freude, and J. Leuthold, "26 Tbit/s line-rate super-channel transmission utilizing all-optical fast Fourier transform processing," *Nature Photonics*, vol. 5, no. 6, pp. 364–371, 2011.

[113] T. Kobayashi, T. Sueta, Y. Cho, and Y. Matsuo, "High-repetition-rate optical pulse generator using a Fabry-Perot electro-optic modulator," *Applied Physics Letters*, vol. 21, no. 8, pp. 341–343, 1972.

[114] T. Kobayashi, H. Yao, K. Amano, Y. Fukushima, A. Morimoto, and T. Sueta, "Optical pulse compression using high-frequency electrooptic phase modulation," *IEEE Journal of Quantum Electronics*, vol. 24, no. 2, pp. 382–387, 1988.

[115] A. J. Metcalf, V. Torres-Company, D. E. Leaird, and A. M. Weiner, "High-Power Broadly Tunable Electrooptic Frequency Comb Generator," *IEEE Journal of Selected Topics in Quantum Electronics*, vol. 19, no. 6, pp. 231–236, 2013.

[116] W. Mao, P. A. Andrekson, and J. Toulouse, "Investigation of a spectrally flat multi-wavelength DWDM source based on optical phase- and intensity-modulation," *Optical Fiber Communication Conference (OFC)*, p. MF78, 2004.

[117] P. Delfyett, S. Gee, Myoung-Taek Choi, H. Izadpanah, Wangkuen Lee, S. Ozharar, F. Quinlan, and T. Yilmaz, "Optical frequency combs from semiconductor lasers and applications in ultrawideband signal processing and communications," *Journal of Lightwave Technology*, vol. 24, no. 7, pp. 2701–2719, 2006.

[118] Y. Ben M'Sallem, Q. T. Le, L. Bramerie, Q.-T. Nguyen, E. Borgne, P. Besnard, A. Shen, F. Lelarge, S. LaRochelle, L. A. Rusch, and J.-C. Simon, "Quantum-Dash Mode-Locked Laser as a Source for 56-Gb/s

DQPSK Modulation in WDM Multicast Applications," *IEEE Photonics Technology Letters*, vol. 23, no. 7, pp. 453–455, 2011.

[119] P. Marin, J. Pfeifle, J. N. Kemal, S. Wolf, K. Vijayan, N. Chimot, A. Martinez, A. Ramdane, F. Lelarge, W. Freude, and C. Koos, "8.32 Tbit/s coherent transmission using a quantum-dash mode-locked laser diode," in *Conference on Lasers and Electro-Optics (CLEO)*, 2016.

[120] J. N. Kemal, P. Marin-Palomo, K. Merghem, G. Aubin, C. Calo, R. Brenot, F. Lelarge, A. Ramdane, S. Randel, W. Freude, and C. Koos, "32QAM WDM Transmission Using a Quantum-Dash Passively Mode-Locked Laser with Resonant Feedback," in *Optical Fiber Communication Conference (OFC)*, 2017, p. Th5C.3.

[121] F. C. Cruz, "Optical frequency combs generated by four-wave mixing in optical fibers for astrophysical spectrometer calibration and metrology," *Optics Express*, vol. 16, no. 17, pp. 13 267–13 275, 2008.

[122] R. Holzwarth, T. Udem, T. W. Hänsch, J. C. Knight, W. J. Wadsworth, and P. S. J. Russell, "Optical Frequency Synthesizer for Precision Spectroscopy," *Physical Review Letters*, vol. 85, no. 11, pp. 2264–2267, 2000.

[123] B. P. Kuo, E. Myslivets, V. Ataie, E. G. Temprana, N. Alic, and S. Radic, "Wideband Parametric Frequency Comb as Coherent Optical Carrier," *Journal of Lightwave Technology*, vol. 31, no. 21, pp. 3414–3419, 2013.

[124] V. Ataie, E. Temprana, L. Liu, E. Myslivets, B. P.-P. Kuo, N. Alic, and S. Radic, "Ultrahigh Count Coherent WDM Channels Transmission Using Optical Parametric Comb-Based Frequency Synthesizer," *Journal of Lightwave Technology*, vol. 33, no. 3, pp. 694–699, 2015.

[125] R. Slavik, S. G. Farwell, M. J. Wale, and D. J. Richardson, "Compact Optical Comb Generator Using InP Tunable Laser and Push-Pull Modulator," *IEEE Photonics Technology Letters*, vol. 27, no. 2, pp. 217–220, 2015.

[126] C. Weimann, P. C. Schindler, R. Palmer, S. Wolf, D. Bekele, D. Korn, J. Pfeifle, S. Koeber, R. Schmogrow, L. Alloatti, D. Elder, H. Yu, W. Bogaerts, L. R. Dalton, W. Freude, J. Leuthold, and C. Koos, "Silicon-organic hybrid (SOH) frequency comb sources for terabit/s data transmission," *Optics Express*, vol. 22, no. 3, pp. 3629–3637, 2014.

[127] G.-H. Duan, A. Shen, A. Akrout, F. V. Dijk, F. Lelarge, F. Pommereau, O. LeGouezigou, J.-G. Provost, H. Gariah, F. Blache, F. Mallecot,

K. Merghem, A. Martinez, and A. Ramdane, “High performance InP-based quantum dash semiconductor mode-locked lasers for optical communications,” *Bell Labs Technical Journal*, vol. 14, no. 3, pp. 63–84, 2009.

[128] T. J. Kippenberg, R. Holzwarth, and S. A. Diddams, “Microresonator-Based Optical Frequency Combs,” *Science*, vol. 332, no. 6029, pp. 555–559, 2011.

[129] J. Pfeifle, V. Brasch, M. Lauermann, Y. Yu, D. Wegner, T. Herr, K. Hartinger, P. Schindler, J. Li, D. Hillerkuss, R. Schmogrow, C. Weimann, R. Holzwarth, W. Freude, J. Leuthold, T. J. Kippenberg, and C. Koos, “Coherent terabit communications with microresonator Kerr frequency combs,” *Nature Photonics*, vol. 8, no. 5, pp. 375–380, 2014.

[130] J. Pfeifle, A. Coillet, R. Henriet, K. Saleh, P. Schindler, C. Weimann, W. Freude, I. V. Balakireva, L. Larger, C. Koos, and Y. K. Chembo, “Optimally Coherent Kerr Combs Generated with Crystalline Whispering Gallery Mode Resonators for Ultrahigh Capacity Fiber Communications,” *Physical Review Letters*, vol. 114, no. 9, p. 093902, 2015.

[131] P. Marin-Palomo, J. N. Kemal, M. Karpov, A. Kordts, J. Pfeifle, M. H. P. Pfeiffer, P. Trocha, S. Wolf, V. Brasch, M. H. Anderson, R. Rosenberger, K. Vijayan, W. Freude, T. J. Kippenberg, and C. Koos, “Microresonator-based solitons for massively parallel coherent optical communications,” *Nature*, vol. 546, no. 7657, pp. 274–279, 2017.

[132] A. Fülöp, M. Mazur, A. Lorences-Riesgo, T. A. Eriksson, P.-H. Wang, Y. Xuan, D. E. Leaird, M. Qi, P. A. Andrekson, A. M. Weiner, and V. Torres-Company, “Long-haul coherent communications using microresonator-based frequency combs,” *Optics Express*, vol. 25, no. 22, pp. 26 678–26 688, 2017.

[133] A. Fülöp, M. Mazur, A. Lorences-Riesgo, Ó. B. Helgason, P.-H. Wang, Y. Xuan, D. E. Leaird, M. Qi, P. A. Andrekson, A. M. Weiner, and V. Torres-Company, “High-order coherent communications using mode-locked dark-pulse Kerr combs from microresonators,” *Nature Communications*, vol. 9, no. 1, p. 1598, 2018.

[134] M. Mazur, M.-G. Suh, A. Fülöp, J. Schröder, V. Torres-Company, M. Karlsson, K. J. Vahala, and P. A. Andrekson, “Enabling high spectral efficiency coherent superchannel transmission with soliton microcombs,” 2018. [Online]. Available: http://arxiv.org/abs/1812.11046

[135] Y. Takushima, H. Sotobayashi, M. E. Grein, E. P. Ippen, and H. A. Haus, "Linewidth of mode combs of passively and actively mode-locked semiconductor laser diodes," in *Optics East*, 2004, pp. 213–227.

[136] G. Vedala, M. Al-Qadi, M. O'Sullivan, J. Cartledge, and R. Hui, "Phase noise characterization of a QD-based diode laser frequency comb," *Optics Express*, vol. 25, no. 14, pp. 15 890–15 904, 2017.

[137] A. Ishizawa, T. Nishikawa, A. Mizutori, H. Takara, A. Takada, T. Sogawa, and M. Koga, "Phase-noise characteristics of a 25-GHz-spaced optical frequency comb based on a phase- and intensity-modulated laser," *Optics Express*, vol. 21, no. 24, pp. 29 186–29 194, 2013.

[138] A. Lorences-Riesgo, M. Mazur, T. A. Eriksson, P. A. Andrekson, and M. Karlsson, "Self-homodyne 24×32-QAM superchannel receiver enabled by all-optical comb regeneration using brillouin amplification," *Optics Express*, vol. 24, no. 26, pp. 29 714–29 723, 2016.

[139] V. Torres-Company and A. M. Weiner, "Optical frequency comb technology for ultra-broadband radio-frequency photonics," *Laser & Photonics Reviews*, vol. 8, no. 3, pp. 368–393, 2014.

[140] B. Kolner, "Space-time duality and the theory of temporal imaging," *IEEE Journal of Quantum Electronics*, vol. 30, no. 8, pp. 1951–1963, 1994.

[141] V. Torres-Company, J. Lancis, and P. Andrés, "Lossless equalization of frequency combs," *Optics Letters*, vol. 33, no. 16, p. 1822, 2008.

[142] R. Krahenbuhl and M. Howerton, "Investigations on short-path-length high-speed optical modulators in LiNbO3 with resonant-type electrodes," *Journal of Lightwave Technology*, vol. 19, no. 9, pp. 1287–1297, 2001.

[143] D. V. Souto, B.-E. Olsson, C. Larsson, and D. A. A. Mello, "Joint-Polarization and Joint-Subchannel Carrier Phase Estimation for 16-QAM Optical Systems," *Journal of Lightwave Technology*, vol. 30, no. 20, pp. 3185–3191, 2012.

[144] D. S. Millar, R. Maher, D. Lavery, T. Koike-Akino, M. Pajovic, A. Alvarado, M. Paskov, K. Kojima, K. Parsons, B. C. Thomsen, S. J. Savory, and P. Bayvel, "Design of a 1 Tb/s Superchannel Coherent Receiver," *Journal of Lightwave Technology*, vol. 34, no. 6, pp. 1453–1463, 2016.

[145] N. K. Fontaine, R. P. Scott, L. Zhou, F. M. Soares, J. P. Heritage, and S. J. B. Yoo, "Real-time full-field arbitrary optical waveform measurement," *Nature Photonics*, vol. 4, no. 4, pp. 248–254, 2010.

[146] A. Lorences-Riesgo, T. A. Eriksson, A. Fülöp, P. A. Andrekson, and M. Karlsson, "Frequency-Comb Regeneration for Self-Homodyne Superchannels," *Journal of Lightwave Technology*, vol. 34, no. 8, pp. 1800–1806, 2016.

[147] M. Mazur, A. Lorences-Riesgo, J. Schröder, P. A. Andrekson, and M. Karlsson, "10 Tb/s PM-64QAM Self-Homodyne Comb-Based Superchannel Transmission with 4% Shared Pilot Tone Overhead," *Journal of Lightwave Technology*, vol. 36, no. 16, pp. 3176–3184, 2018.

[148] K. Mori, F. Hamaoka, K. Horikoshi, and M. Fukutoku, "Stable WDM-Signal-and-LO-frequency Synchronisation and Transmission Employing Multi-Carrier Light Sources and a Multi-Core Fibre for Coherent Photonic Networks," in *European conference on optical communication (ECOC)*, 2016, pp. 202–204.

[149] M. Mazur, A. Lorences-Riesgo, J. Schröder, P. A. Andrekson, and M. Karlsson, "High Spectral Efficiency PM-128QAM Comb-Based Superchannel Transmission Enabled by a Single Shared Optical Pilot Tone," *Journal of Lightwave Technology*, vol. 36, no. 6, pp. 1318–1325, 2018.

[150] P. J. Winzer, "Making spatial multiplexing a reality," *Nature Photonics*, vol. 8, no. 5, pp. 345–348, 2014.

[151] D. J. Richardson, "Filling the Light Pipe," *Science*, vol. 330, no. 6002, pp. 327–328, 2010.

[152] D. Soma, Y. Wakayama, S. Beppu, S. Sumita, T. Tsuritani, T. Hayashi, T. Nagashima, M. Suzuki, H. Takahashi, K. Igarashi, I. Morita, and M. Suzuki, "10.16 Peta-bit/s Dense SDM/WDM transmission over Low-DMD 6-Mode 19-Core Fibre Across C+L Band," in *European Conference on Optical Communication (ECOC)*, 2017.

[153] G. Rademacher, R. S. Luís, B. J. Puttnam, T. A. Eriksson, E. Agrell, R. Maruyama, K. Aikawa, H. Furukawa, Y. Awaji, and N. Wada, "159 Tbit/s C+L Band Transmission over 1045 km 3-Mode Graded-Index Few-Mode Fiber," in *Optical Fiber Communication Conference (OFC)*, 2018, p. Th4C.4.

[154] S. Iano, T. Sato, S. Sentsui, T. Kuroha, and Y. Nishimura, "Multicore optical fiber," in *Optical Fiber Communication Conference (OFC)*, 1979, p. WB1.

[155] S. Berdagué and P. Facq, "Mode division multiplexing in optical fibers," *Applied Optics*, vol. 21, no. 11, p. 1950, 1982.

[156] R. Ryf, J. C. Alvarado, B. Huang, J. Antonio-Lopez, S. H. Chang, N. K. Fontaine, H. Chen, R.-J. Essiambre, E. Burrows, and R. Amezcua-Correa, "Long-distance transmission over coupled-core multicore fiber," *European Conference on Optical Communication (ECOC)*, 2016.

[157] K. S. Abedin, J. M. Fini, T. F. Thierry, V. R. Supradeepa, B. Zhu, M. F. Yan, L. Bansal, E. M. Monberg, and D. J. DiGiovanni, "Multicore Erbium Doped Fiber Amplifiers for Space Division Multiplexing Systems," *Journal of Lightwave Technology*, vol. 32, no. 16, pp. 2800–2808, 2014.

[158] B. J. Puttnam, J. Sakaguchi, J. M. D. Mendinueta, W. Klaus, Y. Awaji, N. Wada, A. Kanno, and T. Kawanishi, "Investigating self-homodyne coherent detection in a 19 channel space-division-multiplexed transmission link," *Optics Express*, vol. 21, no. 2, pp. 1561–1566, 2013.

[159] R. G. H. van Uden, C. M. Okonkwo, V. A. J. M. Sleiffer, M. Kuschnerov, H. De Waardt, and A. M. J. Koonen, "Single DPLL joint carrier phase compensation for few-mode fiber transmission," *IEEE Photonics Technology Letters*, vol. 25, no. 14, pp. 1381–1384, 2013.

[160] B. J. Puttnam, R. S. Luís, G. Rademacher, A. Alfredsson, W. Klaus, J. Sakaguchi, Y. Awaji, E. Agrell, and N. Wada, "Characteristics of homogeneous multi-core fibers for SDM transmission," *APL Photonics*, vol. 4, no. 2, p. 022804, 2019.

[161] O. Golani, D. Pilori, G. Bosco, and M. Shtaif, "Correlated Non-Linear Phase Noise in Multi-Subcarrier Systems," 2018. [Online]. Available: http://arxiv.org/abs/1812.07502

[162] B. Foo, B. Corcoran, and A. J. Lowery, "Distributed Nonlinear Compensation Using Optoelectronic Circuits," *Journal of Lightwave Technology*, vol. 36, no. 6, pp. 1326–1339, 2018.

[163] T. K. Chiang, N. Kagi, T. Fong, M. Marhic, and L. Kazovsky, "Cross-phase modulation in dispersive fibers: theoretical and experimental investigation of the impact of modulation frequency," *IEEE Photonics Technology Letters*, vol. 6, no. 6, pp. 733–736, 1994.

[164] T.-K. Chiang, N. Kagi, M. Marhic, and L. Kazovsky, "Cross-phase modulation in fiber links with multiple optical amplifiers and dispersion compensators," *Journal of Lightwave Technology*, vol. 14, no. 3, pp. 249–260, 1996.

[165] R. Noé, "Phase noise-tolerant synchronous QPSK/BPSK baseband-type intradyne receiver concept with feedforward carrier recovery," *Journal of Lightwave Technology*, vol. 23, no. 2, pp. 802–808, 2005.

[166] M. Qiu, Q. Zhuge, Y. Gao, W. Wang, F. Zhang, and D. Plant, "Cycle Slip Mitigation with Joint Carrier Phase Recovery in Coherent Subcarrier Multiplexing Systems," in *Optical Fiber Communication Conference (OFC)*, 2016, p. Tu3K.2.

[167] M. Kuschnerov, D. van den Borne, K. Piyawanno, F. Hauske, C. Fludger, T. Duthel, T. Wuth, J. Geyer, C. Schulien, B. Spinnler, E.-D. Schmidt, and B. Lankl, "Joint-polarization carrier phase estimation for XPM-limited coherent polarization-multiplexed QPSK transmission with OOK-neighbors," in *European Conference on Optical Communication (ECOC)*, 2008.

[168] F. A. Garcia, D. A. Mello, and H. Waldman, "Feedforward carrier recovery for polarization demultiplexed signals with unequal signal to noise ratios," *Optics Express*, vol. 17, no. 10, pp. 7958–7969, 2009.

[169] C. Liu, J. Pan, T. Detwiler, A. Stark, Y.-T. Hsueh, G.-K. Chang, and S. E. Ralph, "Joint digital signal processing for superchannel coherent optical communication systems," *Optics Express*, vol. 21, no. 7, pp. 8342–8356, 2013.

[170] A. Alfredsson, R. Krishnan, and E. Agrell, "Joint-Polarization Phase-Noise Estimation and Symbol Detection for Optical Coherent Receivers," *Journal of Lightwave Technology*, vol. 34, no. 18, pp. 4394–4405, 2016.

[171] A. F. Alfredsson, E. Agrell, H. Wymeersch, and M. Karlsson, "Phase-Noise Compensation for Spatial-Division Multiplexed Transmission," in *Optical Fiber Communication Conference (OFC)*, 2017, p. Th4C.7.

[172] ——, "Pilot Distributions for Phase Tracking in Space-Division Multiplexed Systems," in *European Conference on Optical Communication (ECOC)*, 2017.

[173] A. F. Alfredsson, E. Agrell, H. Wymeersch, B. J. Puttnam, G. Rademacher, R. S. Luis, and M. Karlsson, "Pilot-Aided Joint-Channel Carrier-Phase

Estimation in Space-Division Multiplexed Multicore Fiber Transmission," *Journal of Lightwave Technology*, 2018.

[174] E. Börjeson, C. Fougstedt, and P. Larsson-Edefors, "ASIC Design Exploration of Phase Recovery Algorithms for M-QAM Fiber-Optic Systems," in *Optical fiber communication conference (OFC)*, 2019, p. W3H.7.

[175] R. S. Luis, B. J. Puttnam, J. M. Delgado Mendinueta, Y. Awaji, and N. Wada, "Impact of spatial channel skew on the performance of spatial-division multiplexed self-homodyne transmission systems," in *International Conference on Photonics in Switching (PS)*, 2015, pp. 37–39.

[176] R. S. Luis, B. J. Puttnam, Y. Awaji, and N. Wada, "OSNR penalties for non-zero skew in space-division multiplexed transmission link with self-homodyne detection," in *Asia Communications and Photonics Conference (ACP)*, 2015, p. ASu5D.5.

[177] T. Miyazaki and F. Kubota, "PSK self-homodyne detection using a pilot carrier for multibit/symbol transmission with inverse-RZ signal," *IEEE Photonics Technology Letters*, vol. 17, no. 6, pp. 1334–1336, 2005.

[178] T. Miyazaki, "Linewidth-tolerant QPSK homodyne transmission using a polarization-multiplexed pilot carrier," *IEEE Photonics Technology Letters*, vol. 18, no. 2, pp. 388–390, 2006.

[179] M. Nakamura, Y. Kamio, and T. Miyazaki, "Linewidth-tolerant 10-Gbit/s 16-QAM transmission using a pilot-carrier based phase-noise cancelling technique," *Optics Express*, vol. 16, no. 14, pp. 10 611–10 616, 2008.

[180] R. S. Luís, B. J. Puttnam, J. M. D. Mendinueta, Y. Awaji, and N. Wada, "Experimental demonstration of a polarization-insensitive self-homodyne detection receiver for optical access," in *European Conference on Optical Communication (ECOC)*, 2015.

[181] D. Che, A. Li, and W. Shieh, "Blind polarization de-multiplexing for Stokes vector direct detection," in *European Conference on Optical Communication (ECOC)*, 2015.

[182] P. Johannisson, M. Sjödin, M. Karlsson, E. Tipsuwannakul, and P. Andrekson, "Cancellation of nonlinear phase distortion in self-homodyne coherent systems," *IEEE Photonics Technology Letters*, vol. 22, no. 11, pp. 802–804, 2010.

[183] M. Sjödin, P. Johannisson, M. Karlsson, Z. Tong, and P. A. Andrekson, "OSNR Requirements for Self-Homodyne Coherent Systems," *IEEE Photonics Technology Letters*, vol. 22, no. 2, pp. 91–93, 2010.

[184] M. Morsy-Osman, Q. Zhuge, L. R. Chen, and D. V. Plant, "Feedforward carrier recovery via pilot-aided transmission for single-carrier systems with arbitrary M-QAM constellations," *Optics Express*, vol. 19, no. 24, pp. 24 331–24 343, 2011.

[185] J. Jignesh, A. Lowery, and B. Corcoran, "Inter-channel nonlinear phase noise compensation using optical injection locking," *Optics Express*, vol. 26, no. 5, pp. 5733–5746, 2018.

[186] R. S. Luís, B. J. Puttnam, J. M. D. Mendinueta, S. Shinada, M. Nakamura, Y. Kamio, and N. Wada, "Digital Self-Homodyne Detection," *IEEE Photonics Technology Letters*, vol. 27, no. 6, pp. 608–611, 2015.

[187] E. Le Taillandier de Gabory, M. Arikawa, Y. Hashimoto, T. Ito, and K. Fukuchi, "A Shared Carrier Reception and Processing Scheme for Compensating Frequency Offset and Phase Noise of Space-Division Multiplexed Signals over Multicore Fibers," in *Optical Fiber Communication Conference (OFC)*, 2013, p. OM2C.2.